10.1177/0003702818780414

Classical Least Squares-Assisted Mid-Infrared (MIR) Laser Spectroscopy Detection of High Explosives on Fabrics

Leonardo C. Pacheco-Londoño[a,b,*], Joaquín Aparicio-Bolaño[a,c], Nataly J. Galán-Freyle[a,b], Andrés D. Román-Ospino[d], Jose L Ruiz-Caballero[a], and Samuel P. Hernandez-Rivera[a*]

[a]ALERT DHS Center of Excellence for Explosives Research, Department of Chemistry, University of Puerto Rico, Mayagüez, PR 00681, USA

[b]School of Basic and Biomedical Sciences, Univ. Simón Bolívar, Barranquilla, Colombia

[c]Department of Chemistry and Physics, University of Puerto Rico, Ponce, PR 00732, USA

[d]Department of Chemistry, University of Puerto Rico, Mayagüez, PR 00681, USA

Corresponding author email addresses: samuel.hernandez3@upr.edu, leonardo.pacheco@upr.edu

Abstract

Mid-infrared (MIR) laser spectroscopy was used to detect the presence of residues of high explosives (HEs) on fabrics. The discrimination of the vibrational signals of HEs from a highly MIR-absorbing substrate was achieved by a simple and fast spectral evaluation without preparation of standards using the classical least squares (CLS) algorithm. CLS focuses on minimizing the differences between the spectral features of the actual spectra acquired using MIR spectroscopy and the spectral features of calculated spectra modeled from linear combinations of the spectra of neat components: HEs, fabrics, and bias. Samples in several combinations of cotton fabrics/HEs were used to validate the methodology. Several experiments were performed focusing on binary, ternary, and quaternary mixtures of TNT, RDX, PETN, and fabrics. The parameters obtained from linear combinations of the calculated spectra were used to perform discrimination analyses and to determine the sensitivity and selectivity of HEs with respect to the substrates and to each other. However, discrimination analysis was not necessary to achieve successful detection of HEs on cotton fabric substrates.

The RDX signals (m_{RDX} > 0.02 mg) on cotton were used to calculate the limit of detection (LOD). The signal-to-noise ratios (S/N) calculated from the spectra of cotton dosed with

decreasing masses of RDX until S/N ≈ 3 resulted in a LOD of 15–33 µg, depending on the vibrational band used. Linear fits generated by comparing the mass dosed RDX with the fraction predicted were also used to calculate the LOD based on the uncertainty of the blank and the slope. This procedure resulted in a LOD of 58 µg. Probably the most representative value of the method LOD was calculated using an interpolation of the P value threshold for low surface dosages of RDX (LOD = 40 µg).

The contribution demonstrates that to achieve HEs detection on fabrics using the proposed algorithm, i.e., determining the presence/absence of HEs on the substrates, the library must contain the spectra of HEs, substrates, and potential interferents or that these spectra be added to the models in the field. If the model does not contain the spectra of the fabric components, there is a high probability of finding false positives for clean samples (no HEs) and a low probability for failed detection in samples with HEs. More work will be required to demonstrate that these new approaches to HE detection work on real-world samples and when contaminating materials are present in the samples.

Keywords: Quantum cascade laser spectroscopy, QCL, high explosives, HEs, classical least squares, CLS, natural and synthetic fabrics, discriminant analysis, DA

Introduction

The remote sensing of chemical residues on substrates using active-mode remote infrared spectroscopy (RIRS)[1–5] depends on various parameters, among which the most important are the excitation energy, the source type, the range (operator-to-target distance), and the angle between the source, target, and detector.[6–10] Other important factors to consider include the reflectivity of the substrates, the surface concentration of the target chemicals, and the optical power of the source. When going into more phenomenological details, attention must be given to surface roughness, effective cross-sectional scattering, and the optical properties of samples and substrates, such as refraction index and extinction coefficient, and the RIRS operational mode used for the measurements, that is, specular or diffuse reflection, transmission, or transflection. In the present study, high explosives (HEs) were deposited onto cotton fabric substrates, which are considered non-ideal substrates because of their low reflectivity and, in principle, have the potential to hinder the characteristic mid-infrared (MIR) bands of HE required for sensing, detection, and subsequent classification and discrimination studies by RIRS. Hence, a large

number of transflected or reflected/scattered photons are required to obtain an optimal signal in the back-reflection setup, such as those generated by an MIR laser source, for example, a quantum cascade laser (QCL), as demonstrated by Faist et al.[11] Other important properties of QCL-based MIR spectrometers are based on the typically small footprint of these devices. Among these properties are field portability, high optical power, room temperature operation,[9] low energy consumption, long-term power stability, and the ability to fine-tune the output frequency.[12] These make QCLs useful for many spectroscopic applications, such as remote sensing of environmental gases and pollutants in the atmosphere,[13] and for critical applications in defense and security.[14–19] The relatively high optical power of at least six orders of magnitude larger than Globar sources (from electrically heated silicon carbide rods) has proven its technological advantages for the development of numerous applications.[8, 20–34]

Quantitative and qualitative spectroscopic analyses have been greatly improved using robust statistical methods. Multivariate analysis methods permit the inclusion of multiple spectral components (wavelengths/wavenumbers), various numbers of samples, and very complex data sets contaminated with spectral noise and spectral overlapping, from which it is possible to predict the sample analyte identities and their concentrations. The diverse multivariate methods available for such tasks, for example, partial least squares regression (PLS), PLS coupled with discriminant analysis (PLS-DA), principal component analysis (PCA), and principal component regression (PCR), have surpassed the 50-year lifetime of classical least squares (CLS), which originated as a univariate analysis method but gradually developed into a multivariate regression algorithm. Moreover, the implementation of CLS-based methods in remote multispectral sensing for image generation from satellite data has served to demonstrate the simplicity of the CLS algorithm and that it can be used in diverse applications in a modern approach.[35] Although in general, it is not straightforward to evaluate the superiority of any given method over another one when analyzing a particular data set, Figueroa-Navedo et al. have recently shown how to establish such comparisons between several multivariate analyses algorithms.[36] In this prior study, the comparisons were based on using laser-induced thermal emission (LITE) data of high explosives in a remotely sensed scenario.

Classical least squares is a well-known regression method that uses the Beer–Bouguer–Lambert linear relation dependence between the absorbance of a chemical species and its molar concentration and is directly applicable to quantitative spectral analyses. The highest goal of

CLS analysis is achieved when a broad spectrum of intensities of several components in a mixture is included in the analysis. This requirement is one of the greatest limitations of CLS, which is that complete knowledge of the individual components in the matrix analyzed is required. Thus, spectra of the mixtures and the spectrum of each neat component are needed to estimate the spectral fraction for each component that is in the composition of the mixture. This is true only when neat components are involved. However, CLS can be considered as the transition state or as a bridge between univariate and multivariate analysis. Accordingly, in CLS, the response at any wavenumber can be considered as a linear combination of the responses of each component that is assumed to be in the mixture. The method also estimates the proportion of each spectrum component in the mixture spectra by minimizing the sum of the squares of the errors. In most cases, this spectral proportion is equal to or linearly proportional to the actual proportion in the mixture. Following this approach, a CLS analysis is presented and discussed.

In the study, binary, ternary, and quaternary mixtures were prepared from the four components in the calibration set: three for the HEs utilized and one for the cotton fabric substrates. A simple implementation of CLS analysis was used for the detection and discrimination analysis of the target HEs by remote sensing with QCL spectroscopy. The CLS methodology and analysis introduces a statistical experimental design based on reference spectra obtained from the pure components included in the mixtures, establishing a simple technique for data visualization and model interpretation. In comparison, PLS-DA-based calibration models require the development of independent models for each substrate surface, or type of fabric and are unsuitable for actual remote-sensing applications. Using the proposed method, in-field actualization of the substrates can be performed, and only the spectra of the neat HEs and surfaces/substrates need to be included in the spectroscopic library.

Experimental

Reagents and Materials

The HEs used in this work were 2,4,6-trinitrotoluene (TNT), pentaerythritol tetranitrate (PETN), and cyclotrimethylenetrinitramine (RDX). PETN and RDX were synthesized in the laboratory. TNT was purchased from Chem Service Inc. Cotton fabric (blue jeans) samples were used as non-reflective, matte substrates.

Sample Preparation

The HE samples were deposited onto the cotton fabric substrates by direct transfer. Two procedures were evaluated for HE deposition. In the first procedure, the desired total amount of HEs or HE mixtures was transferred to a glass Petri dish. Then, the fabric sample was gently rubbed against the bottom of the Petri dish to transfer the HEs by thumbprint pressure. The area covered by the HEs was approximately 2.2×1.7 cm^2. This area was considerably larger than the laser spot area (2×4 mm^2). This finding guaranteed that the total area of the substrate investigated was populated with HEs. In the second deposition procedure, small amounts (particles) of the samples were transferred to the tip of a stainless steel applicator (~1 mm^2 tip area) by pressing against a deposit of HEs or mixture of HEs followed by direct deposition by pressing with the applicator onto the cotton fabric samples. The area covered by the HEs was approximately 0.8 mm^2. This area was much smaller than the laser spot area. Thus, the laser was aimed at the samples in such a way that the particles were located within the laser spot. The fabric was weighed before and after deposition to determine the exact mass of HEs deposited. The weighing was performed on two calibrated scales for appropriate measurement precision. In the first mass determination, a scale with an accuracy of ± 0.1 mg was used for depositions from 0.1 to 3 mg. In the second procedure, a lower-mass quartz balance from a thermal gravimetric analyzer (TGA) with a precision of ± 0.01 mg was used for the smallest amounts of particle deposition (< 0.1 mg). For the two weighing methods used, the fabric was weighed before and after transferring the HE samples.

Instrumentation

A MIR quantum cascade laser- (QCL-) based pre-dispersive spectrometer (LaserScan, Block Engineering,) was used for the spectroscopic measurements. This system was equipped with three synchronized, tunable lasers (tuning ranges: 990 to 1111 cm^{-1}, 1111 to 1178 cm^{-1}, and 1178 to 1600 cm^{-1}). Each diode was scanned for approximately for 0.5 s each for a total scan time of 1.5 s per single, non-co-added run. The average power typically varied from 0.5 to 10 mW across the 600 cm^{-1} tuning range. The other laser parameters were 100:1 polarization (TEM) and a beam divergence of < 2.5 mrad on the *x*-axis and < 5 mrad on the *y*-axis. The instrument was equipped with a 3 in. (7.62 cm) diameter ZnSe lens, which was used to focus the

MIR beam onto the sample and to collect the reflected MIR light and focus it onto the thermoelectrically cooled, internal mercury–cadmium–telluride (MCT) detector. The measurement mode was diffuse reflectance in back reflection (180°) with an experimental setup similar to that of Galan-Freyle, et al.[36] (see Supplemental Material). The wavenumber accuracy and precision were 0.5 cm^{-1} and 0.2 cm^{-1}, respectively. The best operating working distance from the target was 15 ± 3 cm. Each MIR source produced an elliptical laser spot with dimensions of approximately 4 mm x 2 mm at the working distance of 15 cm due to beam divergence differences in the *x–y* plane.

A Q-500 TGA (TA Instruments, Waters LLC) was used for the gravimetric measurements with an accuracy of ± 10 ng and a working temperature range of 20 to 1000 °C. The weighing process was conducted isothermally for each sample at 25 °C for 5 min to achieve thermal stabilization during weighing. This process was undertaken before and after the transfer of the HEs samples.

Results and Discussion

Reference spectra of the HEs and the cotton fabric were acquired by diffuse reflectance using the QCL spectrometer. Roughened gold substrates were used as a background reference for the reflectance measurements. Reflectance units were converted to the negative of the logarithm of the reflectance for spectral display and in preparation for the chemometric analysis to be applied to the data. The spectra of cotton fabric with the corresponding dosing amounts of HEs were acquired in the same form as for the background spectra. Figure 1 shows representative spectra for the HEs and cotton fabric substrates obtained. The normalization was performed using standard normal variate (SNV) as a preprocessing step. SNV was applied to the full spectral region of the analyses to eliminate the baseline drift caused by MIR scattering due to differences in particle size, the topology of the fabric substrate, and the inherent scale of the spectra.

Statistical Model

All spectra were acquired in the Thermo-Galactic Grams/AI SPC spectroscopic file format (Thermo-Fisher Scientific, Inc.) and analyzed using a CLS model developed with customized commands in Matlab (The MathWorks, Inc.) included as part of the Supplemental Material. Spectra were also loaded into the PLS Toolbox v.8.1 (Eigenvector Research, Inc.) to generate the

$$f\left(\mathrm{j}_{j},\hat{\mathrm{b}}_{j}\right)=\hat{\mathrm{b}}_{0}+\hat{\mathrm{b}}_{1}\mathrm{j}_{1}\left(\mathrm{w}_{i}\right)+\ldots\hat{\mathrm{b}}_{j}\mathrm{j}_{j}\left(\mathrm{w}_{i}\right)$$

matrices for other multivariate analyses. Even further statistical analyses were performed using Statgraphics Centurion XV software, version 15.2.05. (Statpoint Technologies, Inc.). The proposed linear model based on CLS can be represented by the following equation:

(1)

where $f\left(\varphi_j,\hat{\beta}_j\right)_i$ represents the *i*th normalized intensity of the spectrum [from –log(R)], calculated from a mixture of several components (*j*); $\varphi_{\mathrm{j}}(\omega_i)$ is the normalized intensity at each wavenumber (ω_i) of the net spectrum belonging to the *j* component and $\hat{\beta}_j$ is a parameter that indicates the fraction or proportion of the net spectrum of a certain component in the spectrum of the mixture. The model assumes that there are no binding interactions among the components in the mixture, which would lead to changes in intensities, band shifts, and the appearance or disappearance of vibrational bands due to binding, physical, or chemical interactions. This implies that the intensity contributions are additive, at least to the first order. The $\hat{\beta}_j$ parameters can be calculated by finding the minimum of the square of the difference between the actual spectra (RS) and the calculated spectra (CS) as follows:

$$d_i = y_i - \hat{f}\left(\varphi_j,\hat{\beta}_j\right)_i$$

(2)

The minimum value of the sum of the squares of d_i (residual) with respect to $\hat{\beta}_j$, illustrated above, can be found by setting to zero the first-order partial derivatives with respect to $\hat{\beta}_j$ and finding the values of $\hat{\beta}_j$. Because the model contains *n* parameters, this generates *n* partial derivative equations that can be represented as follows:

$$\frac{\partial d^2}{\partial \beta_j} = -2\sum_i d_i \frac{\partial f\left(\hat{\varphi}_j,\hat{\beta}_j\right)_i}{\partial \hat{\beta}_j} = 0, \qquad j = 1,2,\cdots,n$$

(3)

It is possible to extract the signals of interest for each component of the mixture from the model. For example, if the component of interest is 1, the extracted spectrum ($\widehat{\Psi}$) is

$$\widehat{\Psi}_{1(\omega_i)} = y_i - \hat{\beta}_0 - \hat{\beta}_2\varphi_2(\omega_i) - \cdots - \hat{\beta}_j\varphi_j(\omega_i) \quad (4)$$

Binary Models

Models for each of the classes (mixtures) studied were generated. Binary-class models were based exclusively on the spectra of cotton fabric substrates and the spectra of each of the HEs. In this case, Eq. 1 reduces to

$$f_{cotton}^{HE} = \hat{\beta}_0 + \hat{\beta}_{cotton}\varphi_{cotton}(\omega_i) + \hat{\beta}_{\mathrm{HE}}\varphi_{\mathrm{HE}}(\omega_i) \quad \textbf{(5)}$$

Twelve loading samples containing various amounts of HEs ranging from 0.1 to 3 mg were deposited on the cotton fabric substrates. The $\hat{\beta}_{\mathrm{HE}}$ parameters were calculated from five replicate spectra acquired at various locations on the substrate surface for samples of several RDX loadings, resulting in a total of 60 spectra. The probability distributions were estimated (see Supplemental Material). Binary models for each of the HE–cotton fabric substrate combinations were generated (P-models). The decision threshold for the model (P) was determined using the predicted average value of $\hat{\beta}_{HEM}$ ($\bar{x}$) for the cotton fabric substrate samples (blank) and the standard deviations (s_d) of the replicates as follows:

$$P = \bar{x} + 3.28\mathrm{x}s_d \quad \textbf{(6)}$$

There is an estimated 5% probability of random error. This probability is based on the definition of the detection limit.[37] There is a high probability that the clean samples are below this threshold. Thus, it was only necessary to have representative spectra of the cotton fabric substrates in the database to generate the discrimination. The models had high sensitivity and selectivity for the HE mass range of 0.1 to 3 mg, as illustrated in Table I. The model was compared with the discriminant analysis (DA). The results are also shown in Table I, where the value of $\hat{\beta}_{HE}$ was used to generate a model for discrimination. The difference between this DA model and the proposed CLS model is that in the calibration the CLS model must be fed with a spectrum of the cotton fabric without HEs (clean substrate) and with the spectra of the neat HEs

and it is not necessary include spectra of the cotton fabric substrates dosed with HEs.

The spectra for the binary models for TNT, RDX, and PETN are shown in Fig. 1a to 1c. In each of these graphs, the spectra with approximately 0.1 mg of HEs deposited on the cotton fabric substrates are shown as blue traces. The predicted spectra from Eq. 5 are shown as red traces. Reference spectra for the powder form of the neat HEs (labeled "Ref") and cotton fabric substrates are shown as black and orange traces, respectively. The HE–cotton spectra with the cotton fabric spectra subtracted using Eq. 5 are shown as green traces. The binary model that consists only of the cotton fabric spectrum and RDX spectrum is presented as an example (the other models are included as part of the Supplemental Material section). The relationship based on Eq. 5 is:

$$f_{cotton}^{RDX} = \hat{\beta}_0 + \hat{\beta}_{cotton}\varphi_{cotton}(\omega_i) + \hat{\beta}_{RDX}\varphi_{RDX}(\omega_i) \quad (7)$$

Figure 2 illustrates the calculation of the probability for RDX in the mass range of 0.1–3 mg as a function of $\hat{\beta}_{RDX}$.

Ternary Models

The equation for ternary models with three components, cotton, TNT, and RDX based on Eq. 1 is as follows:

$$f_{cotton}^{TNT+RDX} = \hat{\beta}_0 + \hat{\beta}_{cotton}\varphi_{cotton}(\omega_i) + \hat{\beta}_{TNT}\varphi_{TNT}(\omega_i) + \hat{\beta}_{RDX}\varphi_{RDX}(\omega_i) \quad \textbf{(8)}$$

Samples of 100% TNT from 0.1 to 3 mg (12 samples), 100% RDX from 0.1 to 3 mg (12 samples), and binary mixtures of 50% TNT/RDX with a total mass ranging from 0.5 to 3 mg (134 samples) were deposited on cotton fabric substrates and processed as in the case of the binary mixtures. The values of the parameters $\hat{\beta}_{TNT}$ and $\hat{\beta}_{RDX}$ were later calculated, and the distribution values for each sample were plotted from Eq. 6. Figure 3 shows that good discrimination for the binary samples was obtained. However, in ternary mixtures, a few samples were classified as binary mixtures composed of TNT–cotton. These samples coincided with the locations on the cotton surface where only small yellow TNT crystals were found when visually inspecting

the samples. The sensitivity and specificity are also shown in Table I. Decision thresholds for the models were determined using the predicted average values ($\bar{x}$) of $\hat{\beta}_{TNT}$ and $\hat{\beta}_{RDX}$ for the cotton fabric samples plus the standard deviation (s_d) times 3.28. In Figure 3, the decision value thresholds are represented by a violet circle with a light-brown border and the thresholds lines are represented by black dotted lines. This threshold was labeled "P" to differentiate it from the DA threshold. This is shown for binary models in the online Supplemental Material.

Quaternary Model

The model for quaternary mixtures of cotton fabric substrates, TNT, RDX, and PETN, and can be described by

$$f_{cotton}^{TNT+RDX+PETN} = \hat{\beta}_0 + \hat{\beta}_{cotton}\varphi_{cotton}(\omega_i) + \hat{\beta}_{TNT}\varphi_{TNT}(\omega_i) + \hat{\beta}_{RDX}\varphi_{RDX}(\omega_i) + \hat{\beta}_{PETN}\varphi_{PETN}(\omega_i) \quad (9)$$

Samples of 100% TNT, 100% RDX, and 100% PETN ranging from 0.1 to 3 mg and samples of mixtures of 50% TNT/RDX, 50% TNT/PETN, 50% PETN/RDX, and 33.3% TNT/PETN/RDX, each with a total mass ranging from 0.5 to 3 mg, were deposited on cotton fabric substrates (252 samples). The values of the parameters $\hat{\beta}_{TNT}$, $\hat{\beta}_{RDX}$, and $\hat{\beta}_{PETN}$ for the mixtures were calculated along with their distribution plot for each sample from the calculated values following Eq. 9. The sensitivity and specificity are also shown in Table I. Visualization of the separation of classes in 3D is difficult for two-dimensional representations. The sensitivity and specificity are also shown in Table I together with the comparison with the DA results.

Tests with Other Substrates

Five other substrates were investigated: white cotton (100%, from a T-shirt), polyester (100%), 65% polyester-35% cotton, 45% polyester-55% cotton, and 84% polyester-16% Spandex. The spectra of neat substrates (free of HE) and the spectra of substrates dosed with TNT were acquired and used for the study. Figure 4 shows the QCL spectra of TNT, polyester, and Spandex used in models for other substrates.

Three models were generated and tested. First, a binary model for TNT based on Eq. 5 was developed. This model was composed of a spectrum for the cotton in blue jeans and a TNT spectrum. The prediction of samples is shown in Table II. All substrates contaminated with TNT were correctly predicted. However, the samples consisting of neat polyester and Spandex (without TNT) were predicted as containing TNT, i.e., as false positives (highlighted in Table II in bold red). The $\hat{\beta}_{TNT}$ values were high for all cases, except for the samples of white cotton substrates, as the model already included a spectrum of cotton from another substrate (blue jeans). Low amounts of TNT (~ 0.1 mg) predicted high $\hat{\beta}_{TNT}$ values. This is unreasonable because the $\hat{\beta}_{TNT}$ values should have been low. However, this can be explained in the cases of the polyester and spandex polymer substrates since both have intense signals in the same spectral window as TNT (see Figure 4).

A second model was built with a spectrum of cotton from blue jeans, a spectrum of polyester and a spectrum of neat TNT. When the spectrum of polyester was added to the model, all the samples with this substrate were correctly predicted with values of $\hat{\beta}_{\mathrm{TNT}}$ near zero. Only the samples that contained Spandex fabric were not correctly classified. Finally, a third model was generated by adding the spectrum of Spandex to the second model. After this, all samples were correctly classified, and the samples with low amounts of TNT (~ 0.1 mg) had a low $\hat{\beta}_{\mathrm{TNT}}$ value (see Table I). Thus, for the classification of samples using CLS and the protocol presented, it is important to include the spectra of all components of the substrate in the model under development to produce a good prediction capability. For the practical identification of HEs on fabrics in defense and security applications, the database to be built must contain the neat spectrum of the HE, as well as the spectra for the substrate fabrics and other components.

Discriminant Analysis for Quaternary Mixtures

To be able to statistically evaluate the discrimination capabilities of the $\hat{\beta}_j$ parameters in the quaternary mixtures and to obtain an improved visualization of the separation

of classes, detailed discriminant analysis was performed using the $\hat{\beta}_j$ parameters as variables. Eight groups were used for the discrimination: cotton fabric substrates, TNT, RDX, PETN, TNT-RDX, TNT-PETN, RDX-PETN, and TNT-RDX-PETN. Two highly significant and statistically weighted discrimination linear functions (F) with respect to the $\hat{\beta}_j$ parameters were obtained. These functions contained nearly all the statistically relevant information because they contributed 95.3% of the discrimination capability of the model. As shown in Table III, two functions with high eigenvalues for the discrimination were highly significant ($p < 0.0001$). In accordance with the canonical correlation coefficient, which represents the ability or effectiveness of the discrimination for new samples, these functions (F1 and F2) showed excellent discrimination to determine group differences, with 93% and 87% confidence levels, respectively. A third function (F3), with a 56% capacity for determining group differences was less effective than functions F1 and F2 but was highly significant ($p < 0.0001$) in the discrimination model. The null hypothesis that the populations have identical discrimination means was tested by the Wilks lambda test. The small value of Wilks' lambda indicates the acceptance of the null hypothesis. The statistical significance was evaluated by the χ^2 p-value (< 0.0001) as illustrated in Table III. It is possible to determine to what extent the contribution of the grouping variable to the variance is explained by the predictor using Wilks' lambda values. Lambda is a measure of the percent variance of independent variables not explained by differences in levels of the independent variable. A small value (near zero) means that there is no variance that is not explained by the independent variable (this is the optimum case). The scale ranges from 0 to 1, where 0 means total discrimination, and 1 means no discrimination, which is determined for each discriminant function to measure the ability to discriminate. The first discriminant function (F1) had a very small Wilks' lambda value (0.02 = 1/50), indicating that approximately one-fiftieth of the variance is not accounted for by group differences. For F2, the Wilks' lambda value was larger (0.17 ≈ 1/6), indicating that approximately one-sixth of the variance is not explained by group differences. In addition, the Wilks' lambda value for F3 was even larger (0.68 =

17/25), indicating that approximately seventeen twenty-fifths of the variance is not explained by in-group differences classification. Figure 5 shows the discriminant plot using the two main functions, F1 and F2. These two principal functions have the capacity to classify the pure HE components on the cotton fiber substrates as PETN, RDX, and TNT. Moreover, the ternary mixtures of TNT/PETN and TNT/RDX on cotton are in the middle of the neat HEs, providing good classification. However, the classification of the ternary mixtures of RDX-PETN/cotton and the quaternary mixtures of TNT-RDX-PETN/cotton could not be accomplished completely by the two main functions F1 and F2. A portion of the RDX-PETN mixtures deposited on cotton fabric substrates were incorrectly classified as having 100% RDX. The same situation occurred for TNT-RDX-PETN mixtures deposited on cotton fabrics. A possible explanation for the lack of discrimination of the RDX-PETN/cotton mixtures is that in some subintervals of the spectral range investigated (e.g., from approximately 1340 to 1402 cm^{-1}), there is a lack of strong PETN absorbance bands, allowing the RDX absorbance signals in these intervals to stand out (see Figure 1d). Therefore, the classification was performed with respect to the RDX/cotton binary component rather than the ternary mixture. The same result is likely to occur in quaternary mixtures (see Supplemental Material). Furthermore, with the consideration of F3 in the analysis and by plotting F1 versus F3 and F2 versus F3, improved classification was achieved for mixtures of RDX/PETN and TNT/RDX/PETN. In this case, the 50% RDX/PETN is in the middle of the two pure components constituting the mixture, and the mixtures of TNT/RDX/PETN are better distributed (see Supplemental Material).

To determine the sensitivity and selectivity values with respect to cotton fabrics, TNT, RDX, and PETN, a binary discriminant analysis (with and without) was performed on each material for the binary, ternary, and quaternary models (see Table I). For the binary models, the sensitivity and selectivity were exact (100%), whereas for the ternary model, these parameters were good, except for the TNT/RDX mixtures. These latter cases should have been classified as containing both RDX and TNT but were ultimately classified as containing only TNT or as containing only RDX. This

could be attributed to a lack of sample homogeneity due to the sample preparation methodology. Similar results were obtained for the quaternary model.

The $\hat{\beta}_j$ values are considered linear proportions of the spectral components in the prediction but no linear behavior is present. However, they are proportional to the concentration of the *j*th component and this is not affected in the detection. The spectra of mixtures are spectra for the amounts of HEs residing on the sampled surface. The intensity of the signals of the HEs depends on the area that the analyte covers on the surface which, in turn, depends on the amount deposited and on the manner in which the material was transferred onto the surface. In the case of HE formulations (two HEs of 50% each; three HEs of 33.33% each), when the samples were deposited on the fabrics, it is possible that some areas of the substrates contained higher amounts of one component than of the others, because it is not possible have homogeneous mixtures of the materials on the substrates with the methodology used for sample deposition. This leads to the situation that some parts of the spectra for the formulations are predicted containing much more material than others, although the HE mixture is a binary formulation or one or two materials in a ternary formulation of HEs. To support the above, a box plot was generated for the ratio of prediction of $\hat{\beta}_{\mathrm{RDX}}/\hat{\beta}_{\mathrm{TNT}}$ (RDX/TNT) in a binary HE mixture (Figure 6a). This ratio should have a value of one but the box plot shows a dispersion values between 0.5 and 2 for the deposited samples in low quantities (~ 0.1 mg) although the distribution is symmetrical. For the other quantities, the distribution is more skewed and less symmetrical. This finding indicates that the binary ratio when depositing the explosive mixture is not retained at all. A comparison is shown between the spectra for 50/50 deposits of low quantities (~ 0.1 mg) and RDX and PETN at two different points on the surface where the value of RDX/PETN differs by 0.5 to 1 in Figure 6b. In this instance, the relative intensities are changed. This indicates there that there are different concentrations of HEs on the individual points sampled on the substrate surface.

Detection of Various Concentrations of Binary Mixtures of HE on Cotton

To determine the levels of the surface concentrations of HEs in binary mixtures on cotton (three component mixtures) that are amenable to quantification using the proposed methodology, four binary mixtures of RDX and PETN were prepared: 5% RDX/95% PETN; 10% RDX/90% PETN; 20% RDX/80% PETN; and 50% RDX/50% PETN. Samples of these mixtures, together with the neat solid forms of

the HEs, were deposited on cotton fabrics and the spectra were acquired. Some of the results of this experiment are shown in Figure 6c. The signals for PETN, RDX, and cotton fabric are clearly observed for the 50% deposits of RDX/PETN, but for the other concentrations, vibrational signatures are not so clearly discernible at first glance. Two spectral subtractions to the spectra of a mixture of PETN/ cotton and RDX/cotton were generated using Eq. 4. These are shown in Figure 6d and Figure 6e, respectively. All signals are observed for the subtraction for PETN and RDX except in the lowest concentration of 5% RDX where these are masked by the spectral noise. This indicates that in the mixture of 5% RDX and 95% PETN it is not possible to identify RDX on the cotton fabric substrate using the proposed methodology.

Limits of Detection (LODs)

The limit of detection (LOD) for RDX/cotton was determined from measurements of several spectra at low analyte amounts (< 0.1 mg). The characteristic MIR vibrational signatures of RDX stood out when applying Eq. 4 to the spectra. Figure 7a shows typical RDX spectra recorded for several masses on the cotton fabric substrates. The reference spectrum of neat RDX (pellet) acquired in the reflectance mode and converted to the negative of the logarithm of reflectance (shown as a solid black line) was used to identify the characteristic bands of RDX and to emphasize the relative signal increase when a greater amount of analyte was deposited on the cotton fabric substrates. New bands were observed at 1085, 1178, and 1484 cm^{-1}. These could be attributed as belonging the dye used in the fabrication of the blue jeans. A spectral subtraction between the cotton fabric from blue jeans and cotton fabric from a 100% rag white T-shirt was carried out using Eq. 4 (see Supplemental Material). This subtraction exposed the signal due to the blue jeans dye, which corresponds to the signals mentioned above.

Three methods for calculating the LOD values were used. In the first method, the signal-to-noise ratios (S/N) were calculated for the 1040 cm^{-1} (C–N–C stretching) and 1463 cm^{-1} (in-plane CH_2 bending) bands[38–41] at each of the nominal deposited RDX masses, as shown in Figure 7b. The improvement in S/N is illustrated for the

two RDX vibrational bands selected as a function of the mass deposited (μg). An S/N value of 3 was found for masses of 15 μg and 33 μg for the signal at 1463 cm^{-1} and 1040 cm^{-1}, respectively, from extrapolation of linear fits. In the second method used, the $\hat{\beta}_{RDX}$ parameter was plotted against the nominal RDX surface mass to find the relationship shown in Figure 7c. The masses, which were measured using an analytical balance and a TGA microbalance, were plotted with respect the beta parameter and linear fits were generated. There is no linear dependence between the $\hat{\beta}_{RDX}$ parameter and the surface mass deposited within the entire mass range. Next, a fit at low mass (measure by the TGA micro-balance) was generated (Figure 7 d). The linear dependence is suitable for the calculated LOD value from the standard deviation of the intercept (S_b) and slope (LOD = $(3\times S_b)$/slope)[42]. The RDX LOD value calculated by this way was 58 μg. In the third method used, an interpolation of the P-value threshold in the fit for low mass was obtained and the mass for this value was 40 μg. This value can be considered the most representative method for the LOD because the P value was calculated based on the definition of LOD. The LOD calculated for the third methodology is the ideal value because it uses the P threshold, which is the one used for the model proposed in this contribution.

Conclusion

The reconceptualization of the CLS algorithm in combination with remote sensing using QCL spectroscopy resulted in the development of a new methodology for the detection of HEs and mixtures of HEs deposited on natural and synthetic fabrics. In this study, the capability of the CLS-assisted MIR laser spectroscopy method for detection of HE in binary, ternary, and quaternary solid mixtures with non-MIR reflective (matte) substrates, such as cotton, polyester, and spandex fabrics, was demonstrated. In addition, if spectra of the neat components, i.e., the HEs of interest (RDX, TNT, and PETN) and spectra of the fabrics are present in the calibration set (or spectroscopic library), it is possible to perform discrimination on surfaces or substrates by updating the model, with the spectra corresponding to the new surface/substrate where the detection would be conducted. This finding was demonstrated using five other substrates: white cotton (100% rag), polyester (100%), 65% polyester/35% cotton, 45% polyester/55% cotton, and

84% polyester/16% spandex. Neat (HE-free) substrates and substrates dosed with TNT were investigated in this experiment. If the model did not contain the spectra of the fabrics, false positives were found for clean samples of HEs and failed detection was found for samples with HEs. Thus, for the methodology to work, the model must contain the spectra for the fabric substrates and HEs.

The RDX signals ($m_{RDX} > 0.02$ mg) on cotton fabrics were used to calculate the method LOD. S/N values calculated from the spectra of cotton fabrics dosed with decreasing masses of RDX until S/N ≈ 3 resulted in an LOD of 15–33 µg, depending on the vibrational band used. Linear fits generated by comparing the dosed RDX mass with the fraction predicted were also used to calculate the LOD based on the uncertainty of the blank and the slope of the fit. This procedure resulted in an LOD of 58 µg. In a third method used to calculate the LOD, using an interpolation of the P value threshold for low RDX dosage resulted in a value of 40 µg. This is probably the most representative value of the method LOD.

Experiments designed to determine the minimum level of quantification of surface concentrations of HEs in ternary mixtures of RDX, PETN, and cotton resulted in a value of 10% RDX. Vibrational signals of both HEs were observed for the subtraction for PETN and RDX except in the lowest concentration of 5% RDX. This indicates that in the mixture of 10% RDX/90% PETN deposited on cotton fabric it was possible to identify RDX on the substrate using the methodology.

The CLS algorithm facilitates the discrimination process upon HE detection and provides a better understanding and better control of the spectral visualization of vibrational signals of interest. There is a priori, nonlinear dependence between the spectrum of the mixture and the spectra of the neat components. It is not possible to quantify the components with the methodology developed, but this nonlinear relationship does not affect the detection in the cases studied. Further research is warranted to demonstrate that this new approach to HE detection works on real-world samples and in the presence of interferents and contaminating materials.

Acknowledgments

This project was part of the outcomes of a Research Experiences for Undergraduates (REU) summer research internship and the 2015 Department of Homeland Security (DHS) Summer Research Teams Programs for Minority-Serving Institutions. The REU summer research

internship was sponsored by the DHS ALERT Center of Excellence for Explosives Research, home-based at Northeastern University, Boston, MA and its R3-C research, development, and education component at the University of Puerto Rico–Mayagüez Campus.

Conflict of Interest

The authors report there are no conflicts of interest.

Funding

This material is based upon work supported by the U.S. Department of Homeland Security, Science and Technology Directorate, Office of University Programs, under Grant Award 2013-ST-061-ED0001. The views and conclusions contained in this document are those of the authors and should not be interpreted as necessarily representing the official policies, either expressed or implied, of the U.S. Department of Homeland Security.

References

1. J.E. Parmeter. “The Challenge of Standoff Explosives Detection”. 38th Annual 2004 International Carnahan Conference on Security Technology, 2004. Pp. 355–358.
2. J.C. Carter, S.M. Angel, M. Lawrence-Snyder, J. Scaffidi, et al. “Standoff Detection of High Explosive Materials at 50 Meters in Ambient Light Conditions Using a Small Raman Instrument”. Appl. Spectrosc. 2005. 59(6): 769–775.
3. W. Ortiz-Rivera, L.C. Pacheco-Londoño, J.R. Castro-Suarez, H. Felix-Rivera, et al. “Vibrational Spectroscopy Standoff Detection of Threat Chemicals”. Proc. SPIE 2011. 8031(803129-803129-803110.
4. J. Moros, J.A. Lorenzo, K. Novotný, J.J. Laserna. “Fundamentals of Stand-Off Raman Scattering Spectroscopy for Explosive Fingerprinting”. J. Raman Spectrosc 2013. 44(1): 121–130.
5. S. Wallin, A. Pettersson, H. Östmark, A. Hobro. “Laser-Based Standoff Detection of Explosives: A Critical Review”. Anal. Bioanal. Chem 2009. 395(2): 259–274.
6. N.J. Galán-Freyle, L.C. Pacheco-Londoño, A.M. Figueroa-Navedo, S.P. Hernandez-Rivera. “Standoff Detection of Highly Energetic Materials Using Laser-Induced Thermal Excitation of Infrared Emission”. Appl. Spectrosc. 2015. 69(5): 535–544.

7. J.R. Castro-Suarez, L.C. Pacheco-Londoño, M. Vélez-Reyes, M. Diem, et al. “FT-IR Standoff Detection of Thermally Excited Emissions of Trinitrotoluene (TNT) Deposited on Aluminum Substrates”. Appl. Spectrosc. 2013. 67(2): 181–186.

8. J. Suter, B. Bernacki, M. Phillips. “Spectral and Angular Dependence of Mid-Infrared Diffuse Scattering from Explosives Residues for Standoff Detection Using External Cavity Quantum Cascade Lasers”. Appl. Phys. B. 2012. 108(4): 965–974.

9. L.C. Pacheco-Londoño, W. Ortiz-Rivera, O.M. Primera-Pedrozo, S.P. Hernández-Rivera. “Vibrational Spectroscopy Standoff Detection of Explosives”. Anal. Bioanal. Chem. 2009. 395(2): 323–335.

10. A. Pettersson, I. Johansson, S. Wallin, M. Nordberg, et al. “Near Real-Time Standoff Detection of Explosives in a Realistic Outdoor Environment at 55 m Distance”. Propellants Explos. Pyrotech 2009. 34(4): 297–306.

11. J. Faist, F. Capasso, D.L. Sivco, C. Sirtori, et al. “Quantum Cascade Laser”. Science 1994. 264(5158): 553–556.

12. L. Hvozdara, N. Pennington, M. Kraft, M. Karlowatz, et al. “Quantum Cascade Lasers for Mid-Infrared Spectroscopy”. Vib. Spectrosc 2002. 30(1): 53–58.

13. P.C. Castillo, I. Sydoryk, B. Gross, F. Moshary. "Ambient Detection of CH_4 and N_2O by Quantum Cascade Laser". Proceedings Volume 8718. Advanced Environmental, Chemical, and Biological Sensing Technologies X. 2013. 87180J. doi: 10.1117/12.2016294.

14. C. Kumar, N. Patel. "Quantum Cascade Lasers and Applications in Defense and Security". Photonics Society Summer Topical Meeting Series, 2011 IEEE. 2011. Pp. 49–50.

15. C. Kumar, N. Patel. “Mid Wave Infrared and Long Wave Infrared QCLs and their Applications to Sensors". Optical Chemical and Biological Sensors II session. Optical Sensors 2013. Rio Grande, Puerto Rico, United States, 14–17 July 2013. Paper SW2B.

16. E. Normand, I. Howieson, M. McCulloch, P. Black. “Quantum Cascade Laser (QCL) Based Sensor for the Detection of Explosive Compounds”. Proc. SPIE 6402, Optics and Photonics for Counterterrorism and Crime Fighting II, 64020G. 28 September 2006. doi: 10.1117/12.695423.

17. C.K.N. Patel. “Laser Based In-Situ and Standoff Detection of Chemical Warfare Agents and Explosives”. Proceedings Volume 7484, Optically Based Biological and Chemical Detection for Defence V. 2009. 748402. doi: 10.1117/12.835883.
18. C.K.N. Patel, A. Lyakh. “High Power Quantum Cascade Lasers for Infrared Countermeasures, Targeting and Illumination, Beacons and Standoff Detection of Explosives and CWAs”. In: Thomas George; Achyut K. Dutta; M. Saif Islam, editors. Micro- and Nanotechnology Sensors, Systems, and Applications VII. Proc. SPIE 9467. 2015. 946702.
19. J.R. Castro-Suarez, M. Hidalgo-Santiago, S.P. Hernández-Rivera. “Detection of Highly Energetic Materials on Non-Reflective Substrates Using Quantum Cascade Laser Spectroscopy”. Appl. Spectrosc. 2015. 69(9): 1023–1035.
20. L. Zhang, G. Tian, J. Li, B. Yu. “Applications of Absorption Spectroscopy Using Quantum Cascade Lasers”. Appl. Spectrosc. 2014. 68(10): 1095–1107.
21. C.W. van Neste, L.R. Senesac, T. Thundat. “Standoff Spectroscopy of Surface Adsorbed Chemicals”. Anal. Chem. 2009. 81(5): 1952–1956.
22. C. Charlton, A. Katzir, B. Mizaikoff. “Infrared Evanescent Field Sensing with Quantum Cascade Lasers and Planar Silver Halide Waveguides”. Anal. Chem. 2005. 77(14): 4398–4403.
23. L. Ciaffoni, G. Hancock, J.J. Harrison, J.-P.H. van Helden, et al. “Demonstration of a Mid-Infrared Cavity Enhanced Absorption Spectrometer for Breath Acetone Detection”:. Anal. Chem. 2012. 85(2): 846–850.
24. J. Kohoutek, A. Bonakdar, R. Gelfand, D. Dey, et al. “Integrated All-Optical Infrared Switchable Plasmonic Quantum Cascade Laser”. Nano Lett. 2012. 12(5): 2537–2541.
25. M.R. Kole, R.K. Reddy, M.V. Schulmerich, M.K. Gelber, et al. “Discrete Frequency Infrared Microspectroscopy and Imaging with a Tunable Quantum Cascade Laser”. Anal. Chem. 2012. 84(23): 10366–10372.
26. B. Lendl, J. Frank, R. Schindler, A. Müller, et al. “Mid-Infrared Quantum Cascade Lasers for Flow Injection Analysis”. Anal. Chem. 2000. 72(7): 1645–1648.
27. A. Mertiri, H. Altug, M.K. Hong, P. Mehta, et al. “Nonlinear Midinfrared Photothermal Spectroscopy Using Zharov Splitting and Quantum Cascade Lasers”. ACS Photonics 2014. 1(8): 696–702.

28. M.A. Pleitez, T. Lieblein, A. Bauer, O. Hertzberg, et al. “In Vivo Noninvasive Monitoring of Glucose Concentration in Human Epidermis by Mid-Infrared Pulsed Photoacoustic Spectroscopy”. Anal. Chem. 2012. 85(2): 1013–1020.

29. A. Rüther, M. Pfeifer, V.A. Lórenz-Fonfría, S. Lüdeke. “pH Titration Monitored by Quantum Cascade Laser-Based Vibrational Circular Dichroism”. J. Phys. Chem. B. 2014. 118(14): 3941–3949.

30. K. Wörle, F. Seichter, A. Wilk, C. Armacost, et al. “Breath Analysis with Broadly Tunable Quantum Cascade Lasers”. Anal. Chem. 2013. 85(5): 2697–2702.

31. K. Yeh, S. Kenkel, J.-N. Liu, R. Bhargava. “Fast Infrared Chemical Imaging with a Quantum Cascade Laser”. Anal. Chem. 2014. 87(1): 485–493.

32. D.C. Grills, A.R. Cook, E. Fujita, M.W. George, et al. “Application of External-Cavity Quantum Cascade Infrared Lasers to Nanosecond Time-Resolved Infrared Spectroscopy of Condensed-Phase Samples Following Pulse Radiolysis”. Appl. Spectrosc. 2010. 64(6): 563–570.

33. E.L. Holthoff, L.S. Marcus, P.M. Pellegrino. “Quantum Cascade Laser Based Photoacoustic Spectroscopy for Depth Profiling Investigations of Condensed-Phase Materials”. Appl. Spectrosc. 2012. 66(9): 987–992.

34. S. Schaden, A. Domínguez-Vidal, B. Lendl. “On-Line Reaction Monitoring in the Liquid Phase Using Two Mid-Infrared Quantum Cascade Lasers Simultaneously”. Appl. Spectrosc. 2006. 60(5): 568–571.

35. N.B. Gallagher, T.A. Blake, P.L. Gassman, J.M. Shaver, et al. “Multivariate Curve Resolution Applied to Infrared Reflection Measurements of Soil Contaminated with an Organophosphorus Analyte”. Appl. Spectrosc. 2006. 60(7): 713–722.

36. N.J. Galán-Freyle, L.C. Pacheco-Londoño, A.D. Román-Ospino, S.P. Hernandez-Rivera. “Applications of Quantum Cascade Laser Spectroscopy in the Analysis of Pharmaceutical Formulations”. Appl. Spectrosc. 2016. 70(9): 1511–1519.

37. J.N. Miller, J.C. Miller. Estadistica y Quimiometria Para Quimica Analitica. Madrid: Prentice Hall, 2002.

38. R. Infante-Castillo, L. Pacheco-Londoño, S.P. Hernández-Rivera. “Vibrational Spectra and Structure of RDX and its 13C- and 15N-Labeled Derivatives: A Theoretical and Experimental Study”. Spectrochim. Acta, Part A. 2010. 76(2): 137–141.

39. R. Infante-Castillo, L.C. Pacheco-Londoño, S.P. Hernández-Rivera. “Monitoring the α→β Solid–Solid Phase Transition of RDX with Raman Spectroscopy: A Theoretical and Experimental Study”. J. Mol. Struct. 2010. 970(1–3): 51–58.

40. J.L. Ruiz-Caballero, J.A. Aparicio-Bolaño, A.M. Figueroa-Navedo, L.C. Pacheco-Londoño, et al. “Optical Properties of β-RDX Thin Films Deposited on Gold and Stainless Steel Substrates Calculated from Reflection–Absorption Infrared Spectra”. Appl. Spectrosc. 2017. 71(8): 1990–2000.

41. A.M. Figueroa-Navedo, J.L. Ruiz-Caballero, L.C. Pacheco-Londoño, S.P. Hernández-Rivera. “Characterization of α- and β-RDX Polymorphs in Crystalline Deposits on Stainless Steel Substrates”. Cryst. Growth Des 2016. 16(7): 3631–3638.

42. G.L. Long, J.D. Winefordner. “Limit of Detection A Closer Look at the IUPAC Definition”. Anal. Chem. 1983. 55(07): 712A–724A.

10.1177/0003702818780414

Figures

Figure 1.

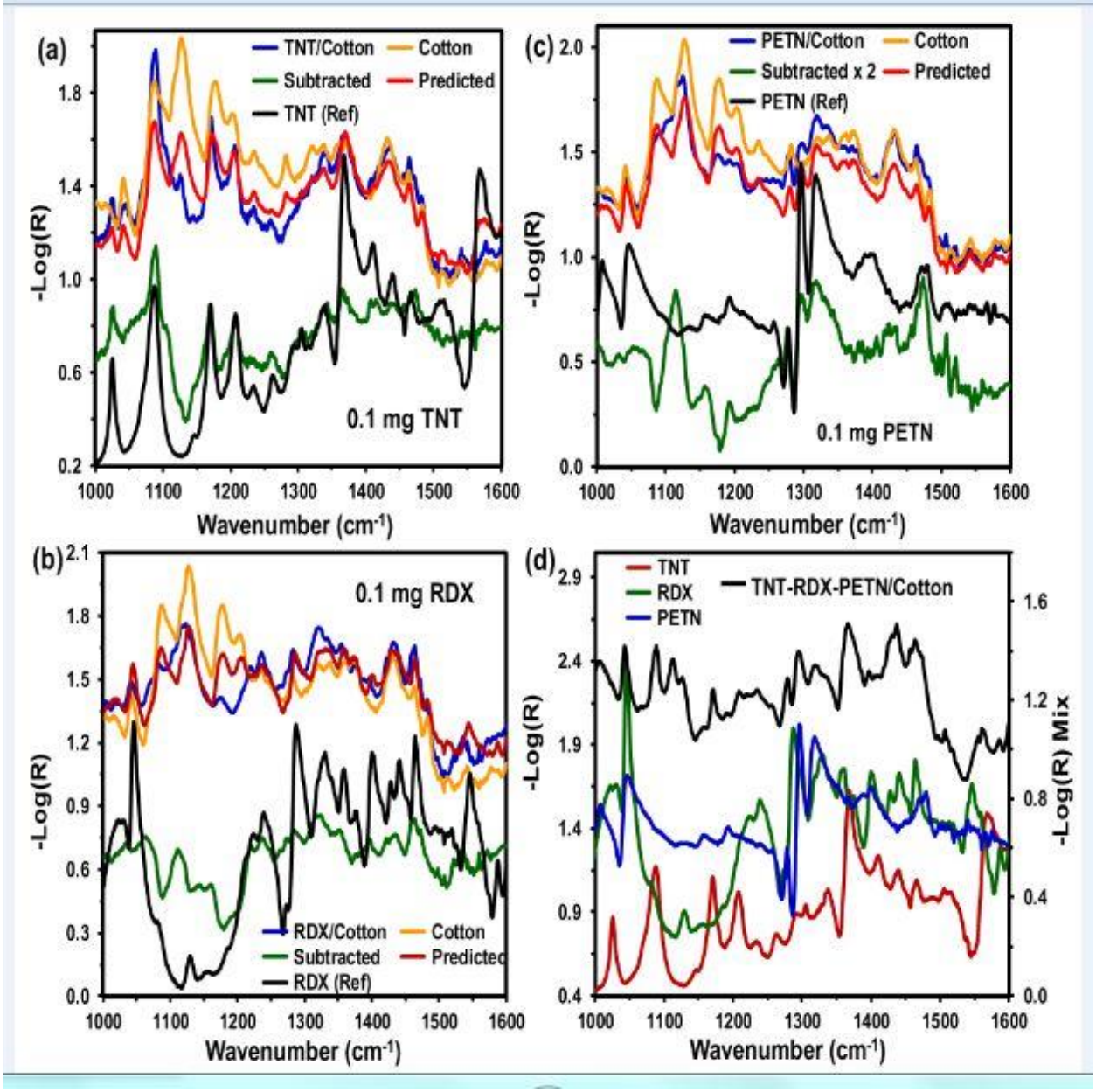

10.1177/0003702818780414

Figure 2.

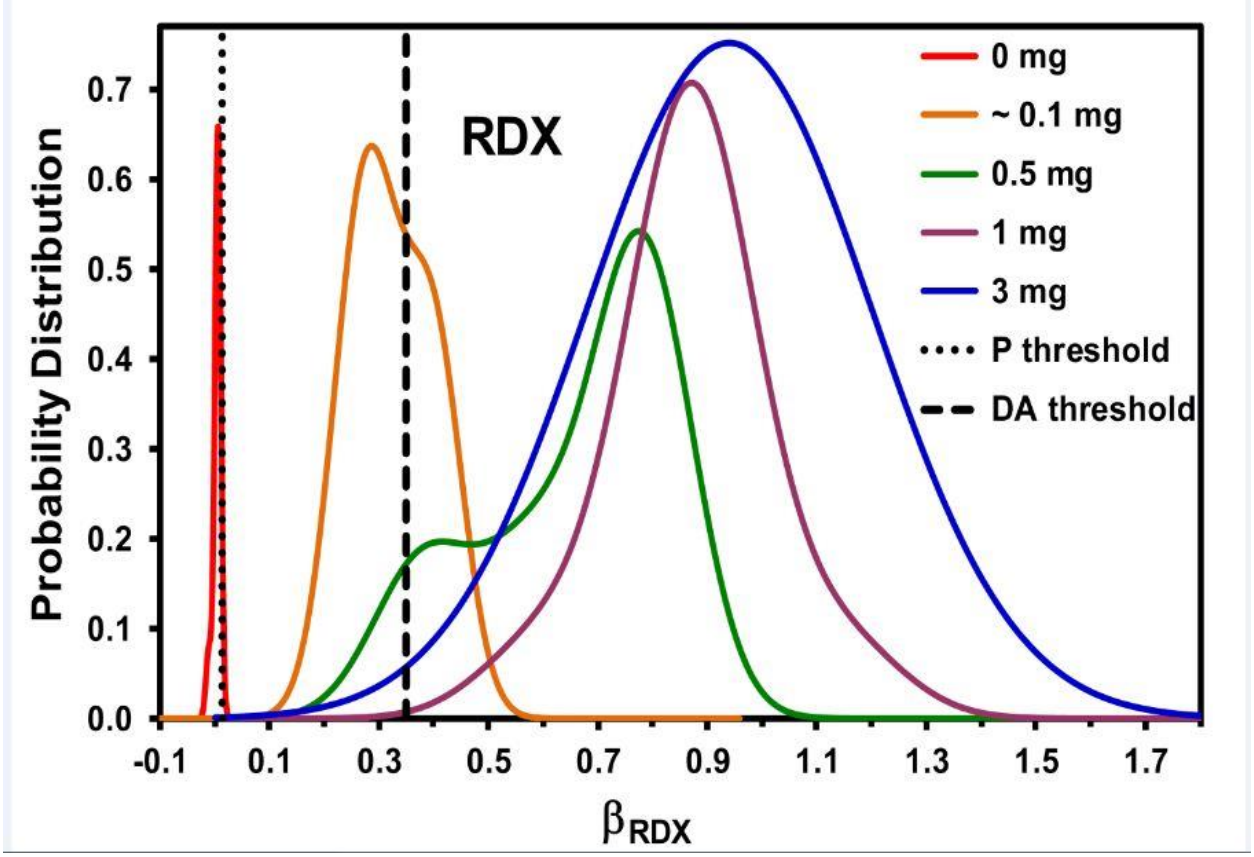

10.1177/0003702818780414

Figure 3.

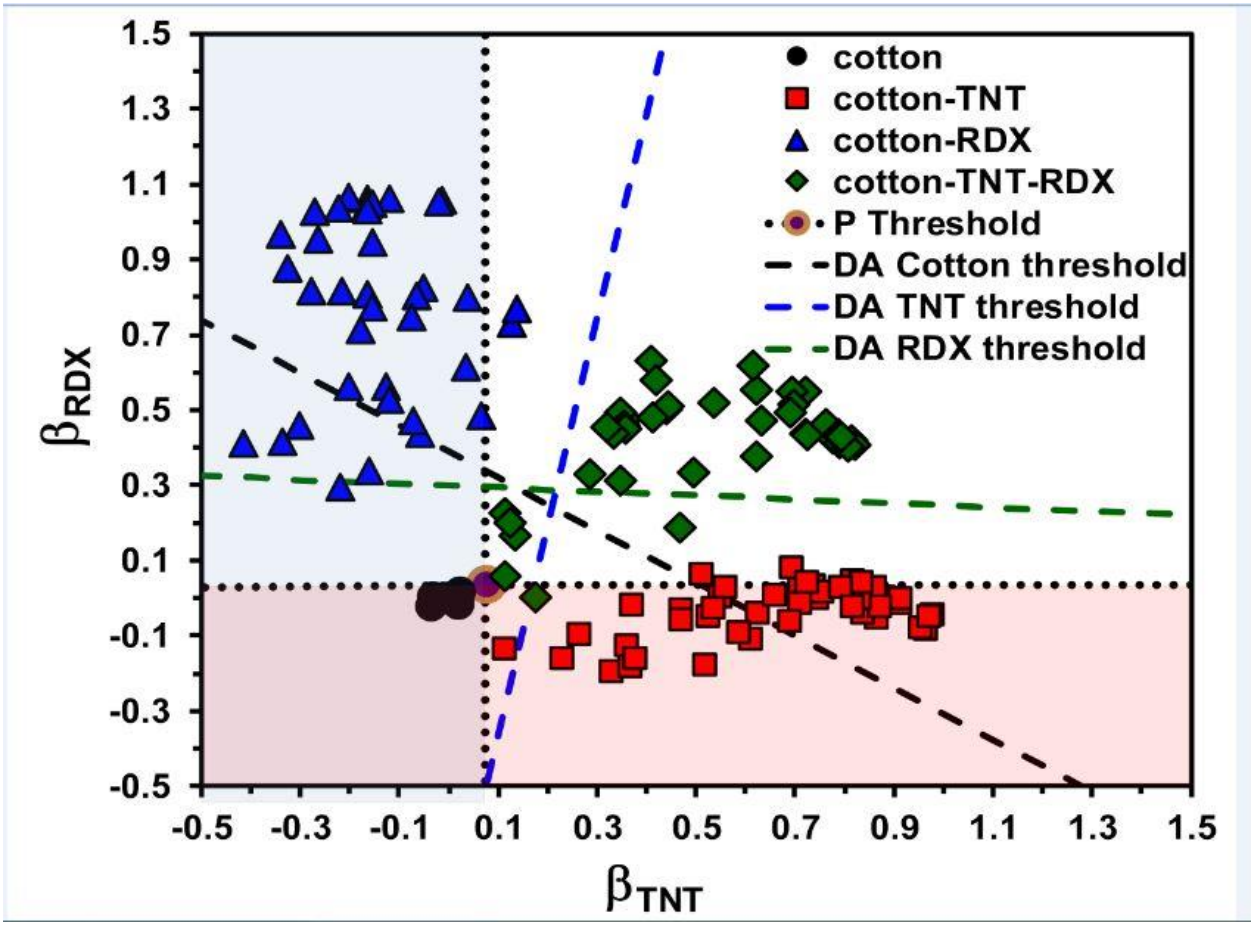

10.1177/0003702818780414

Figure 4.

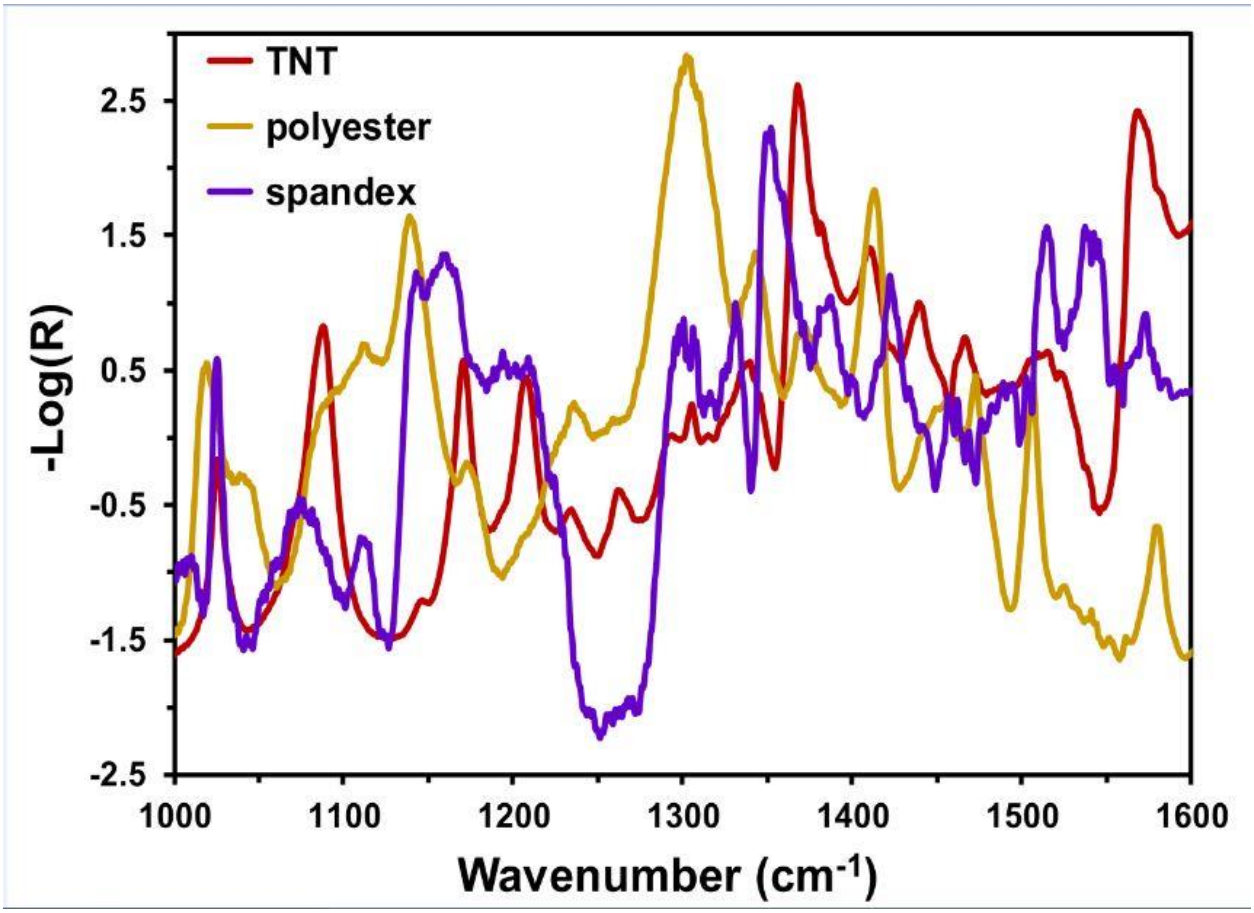

10.1177/0003702818780414

Figure 5.

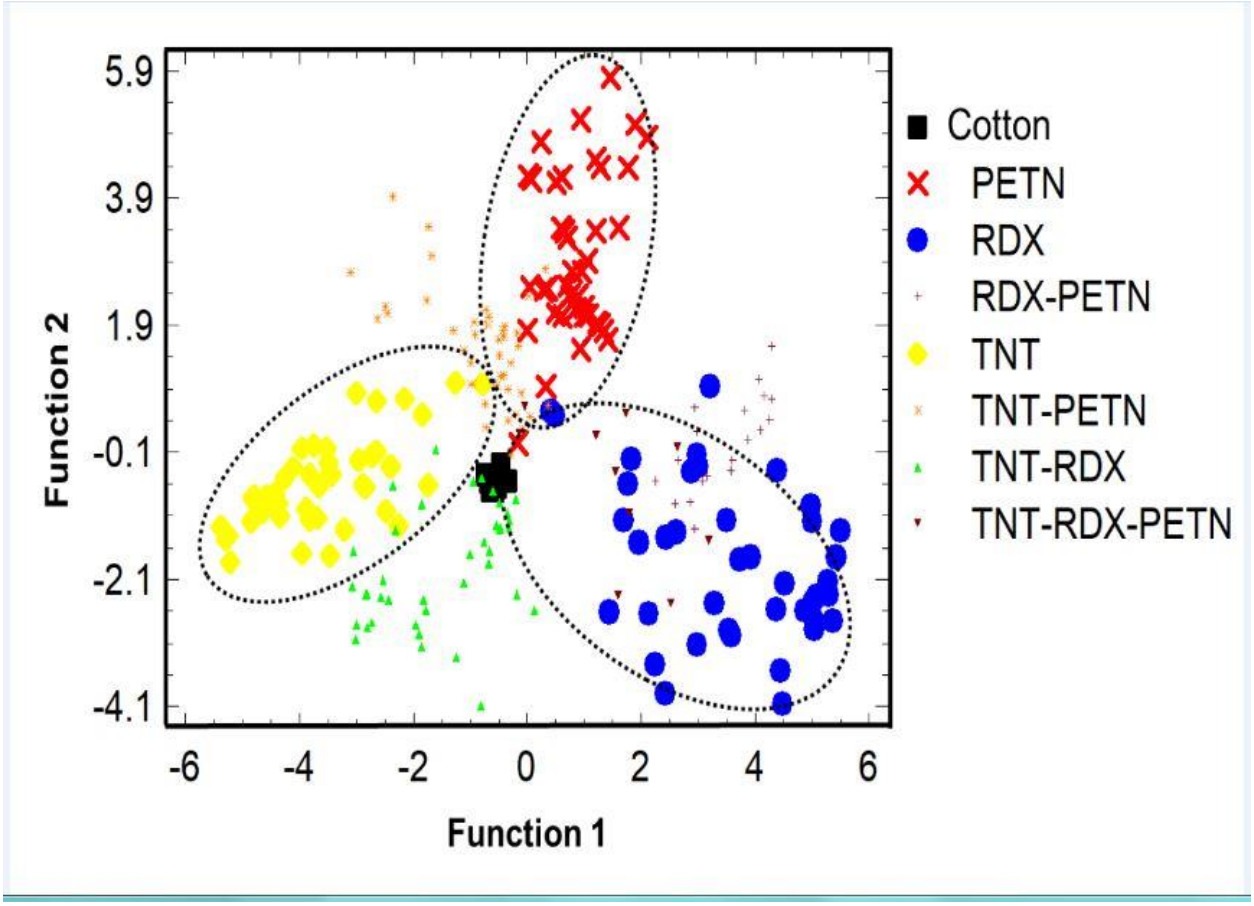

10.1177/0003702818780414

Figure 6.

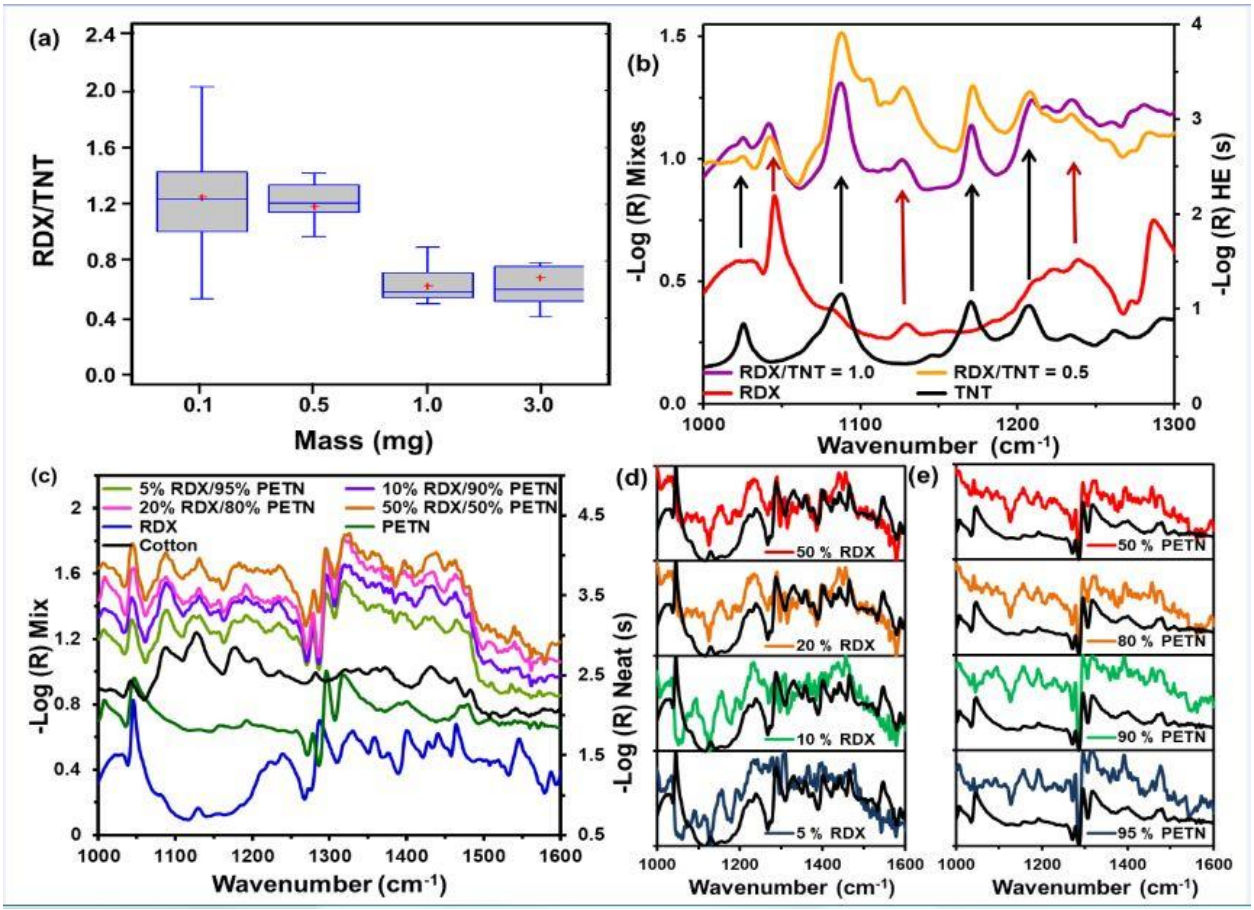

10.1177/0003702818780414

Figure 7.

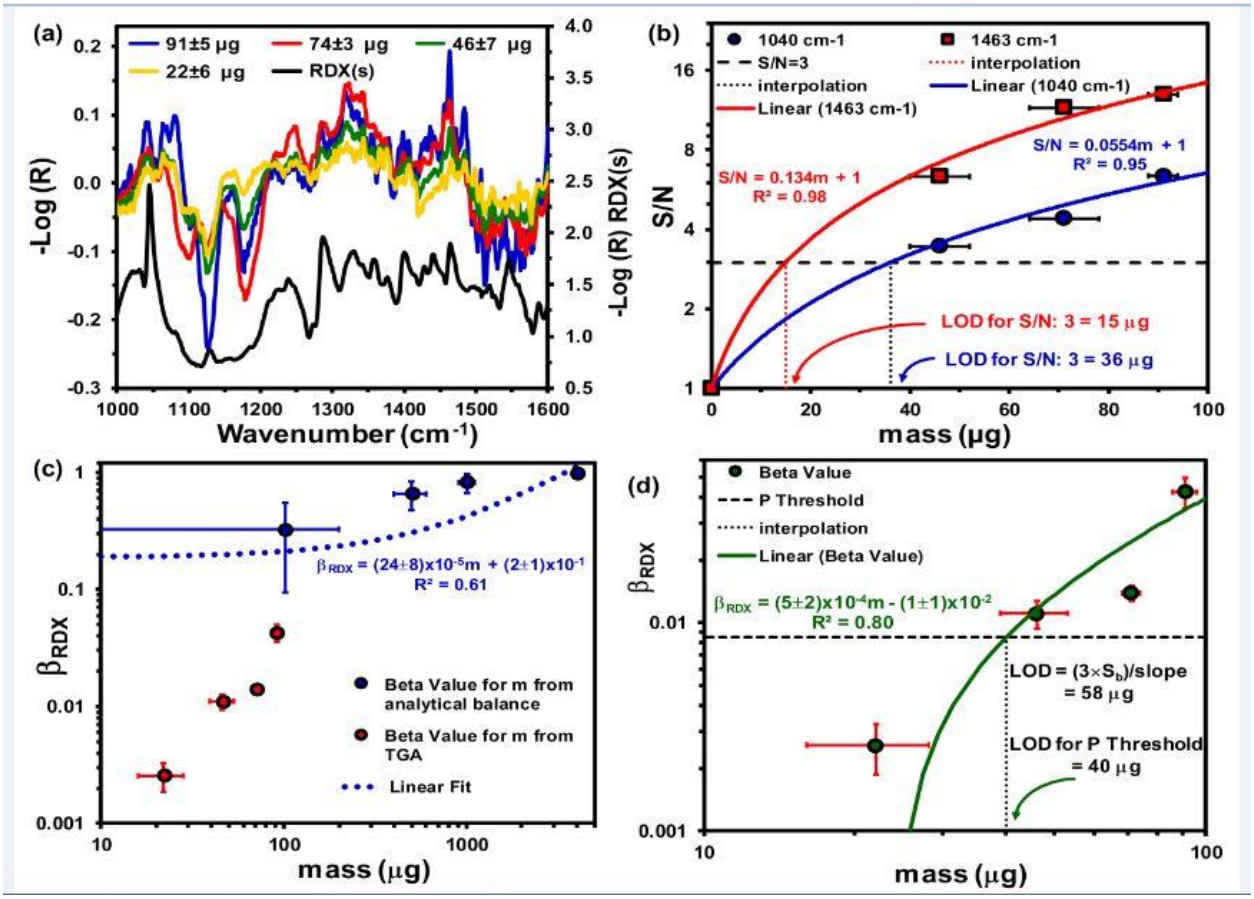

10.1177/0003702818780414

TABLE 1

	Model		Discriminant Model	
	Sensitivity	**Specificity**	**Sensitivity**	**Specificity**
	Binary		**Binary**	
Cotton	100%	100%	100%	89%
TNT	100%	100%	89%	100%
Cotton	100%	100%	100%	85%
RDX	100%	100%	85%	100%
Cotton	100%	100%	100%	95%
PETN	100%	100%	95%	100%
	Ternary		**Ternary**	
Cotton	100%	100%	100%	86%
TNT	100%	97%	94%	100%
RDX	99%	88%	91%	100%
HEM	100%	100%	86%	100%
	Quaternary		**Quaternary**	
Cotton	100%	100%	100%	88%
TNT	89%	94%	86%	90%
RDX	95%	84%	86%	100%
PETN	99%	67%	86%	91%
HEM	100%	100%	88%	100%

10.1177/0003702818780414

Table 2. Prediction of $\widehat{\boldsymbol{\beta}}_{TNT}$ parameters for the three models developed

Sample	Model 1 ($\widehat{\boldsymbol{\beta}}_{TNT}$)	Model 2 ($\widehat{\boldsymbol{\beta}}_{TNT}$)	Model 3 ($\widehat{\boldsymbol{\beta}}_{TNT}$)
white cotton	-0.05 ± 0.01	-0.07 ± 0.01	-0.06 ± 0.01
polyester	**0.15 ±0 .05**	-0.01 ± 0.03	0.00 ± 0.02
65% polyester 35% cotton	**0.15 ± 0.03**	-0.05 ± 0.03	-0.01 ± 0.03
45% polyester 55% cotton	**0.04 ± 0.04**	-0.03 ± 0.03	-0.07 ± 0.03
84% polyester 16% spandex	**0.31 ± 0.03**	**0.17 ± 0.03**	0 ± 0.03
2 mg TNT 65% polyester 35% cotton	0.83 ± 0.04	0.78 ± 0.04	0.68 ± 0.05
0.5 mg TNT 65% polyester 35% cotton	0.5 ± 0.1	0.4 ± 0.1	0.3 ± 0.1
2 mg TNT 45% polyester 55% cotton	0.72 ± 0.08	0.67 ± 0.09	0.58 ± 0.09
0.5 mg TNT 45% polyester 55% cotton	0.38 ± 0.02	0.31 ± 0.02	0.27 ± 0.03
4 mg TNT on 84% polyester 16% spandex	0.9 ± 0.1	0.9 ± 0.1	0.9 ± 0.1
2 mg TNT on 84% polyester 16% spandex	0.3 ± 0.1	0.3 ± 0.2	0.5 ± 0.2
0.8 mg TNT on 84% polyester 16% spandex	0.3 ± 0.2	0.2 ± 0.2	0.3 ± 0.2
0.5 mg TNT on 84% polyester 16% spandex	0.4 ± 0.1	0.3 ± 0.1	0.2 ± 0.2
~0.1 mg TNT on 84% polyester 16% spandex	**0.25 ± 0.01**	**0.12 ± 0.01**	**0.05 ± 0.01**

10.1177/0003702818780414

TABLE 3

Discriminant functions	1	2	3
Eigenvalue	6.2	3.2	0.5
Relative %	63%	32%	5%
Canonical Correlation	0.93	0.87	0.56
Wilks Lambda	0.02	0.16	0.68
Chi-squared	901.9	431.7	90.6
p-value	< 0.0001	< 0.0001	< 0.0001

10.1177/0003702818780414

Supplemental Material

Classical Least Squares-Assisted MIR Laser Spectroscopy Detection of High Explosives on Fabrics

Leonardo C. Pacheco-Londoño[a,b,*], Joaquín Aparicio-Bolaño[a,c], Nataly J. Galán-Freyle[a,b], Andrés D. Román-Ospino[d], Jose L Ruiz-Caballero,[a] and Samuel P. Hernandez-Rivera[a]

[a]ALERT DHS Center of Excellence for Explosives Research, Department of Chemistry, University of Puerto Rico, Mayagüez, PR 00681, USA

[b]School of Basic and Biomedical Sciences, Universidad Simón Bolívar, Barranquilla, Colombia

[c]Department of Chemistry and Physics, University of Puerto Rico, Ponce, PR 00732, USA

[d]Department of Chemistry, University of Puerto Rico, Mayagüez, PR 00681, USA

Corresponding author emails: samuel.hernandez3@upr.edu, leonardo.pacheco@upr.edu

1. Experimental setup used in the investigations

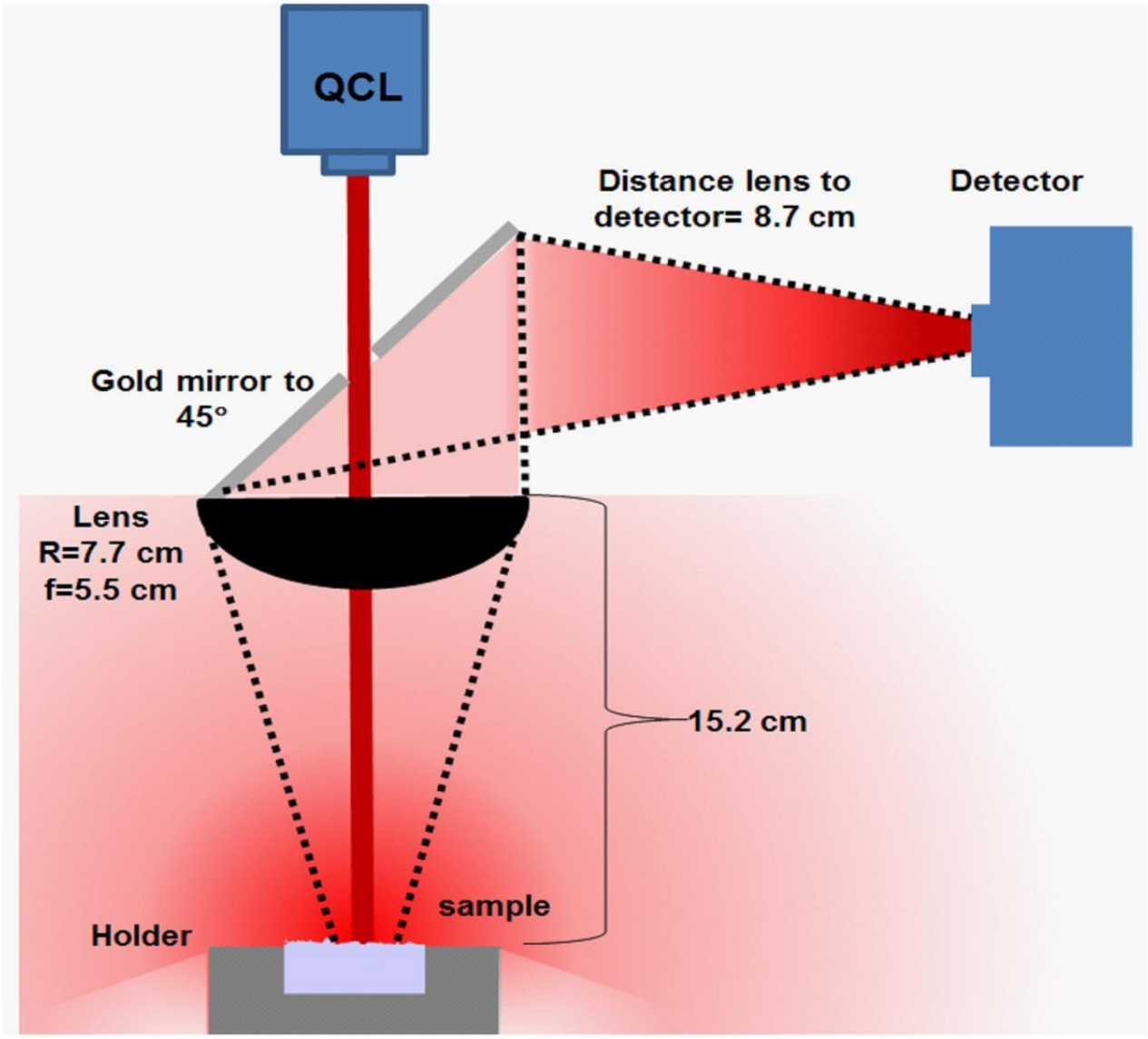

Figure S1. Experimental setup used for the QCL based reflectance measurements.

Figure S2 shows the details of the weighting procedure using the quartz balance of a thermogravimetric analysis (TGA) system.

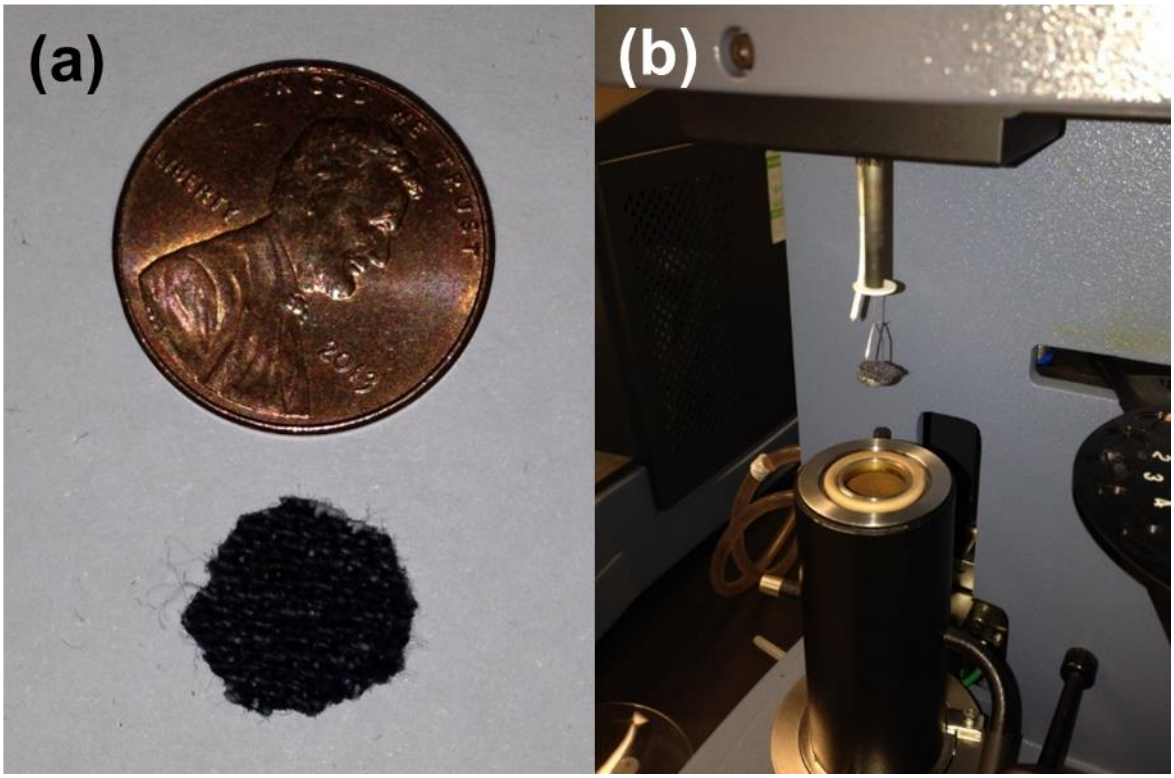

Figure S2. (a) Photograph of cotton fabric from jean used in the experiment; (b) weighting of HE in TGA balance.

2. CLS Binary Model for TNT/cotton

The binary model of TNT/cotton consisted only of spectra of cotton and cotton with TNT. The equation used for the CLS model of the binary mixture is:

$$f_{cotton}^{TNT} = \hat{\beta}_0 + \hat{\beta}_{cotton}\varphi_{cotton}(\omega_i) + \hat{\beta}_{TNT}\varphi_{TNT}(\omega_i) \quad \text{(SM 1)}$$

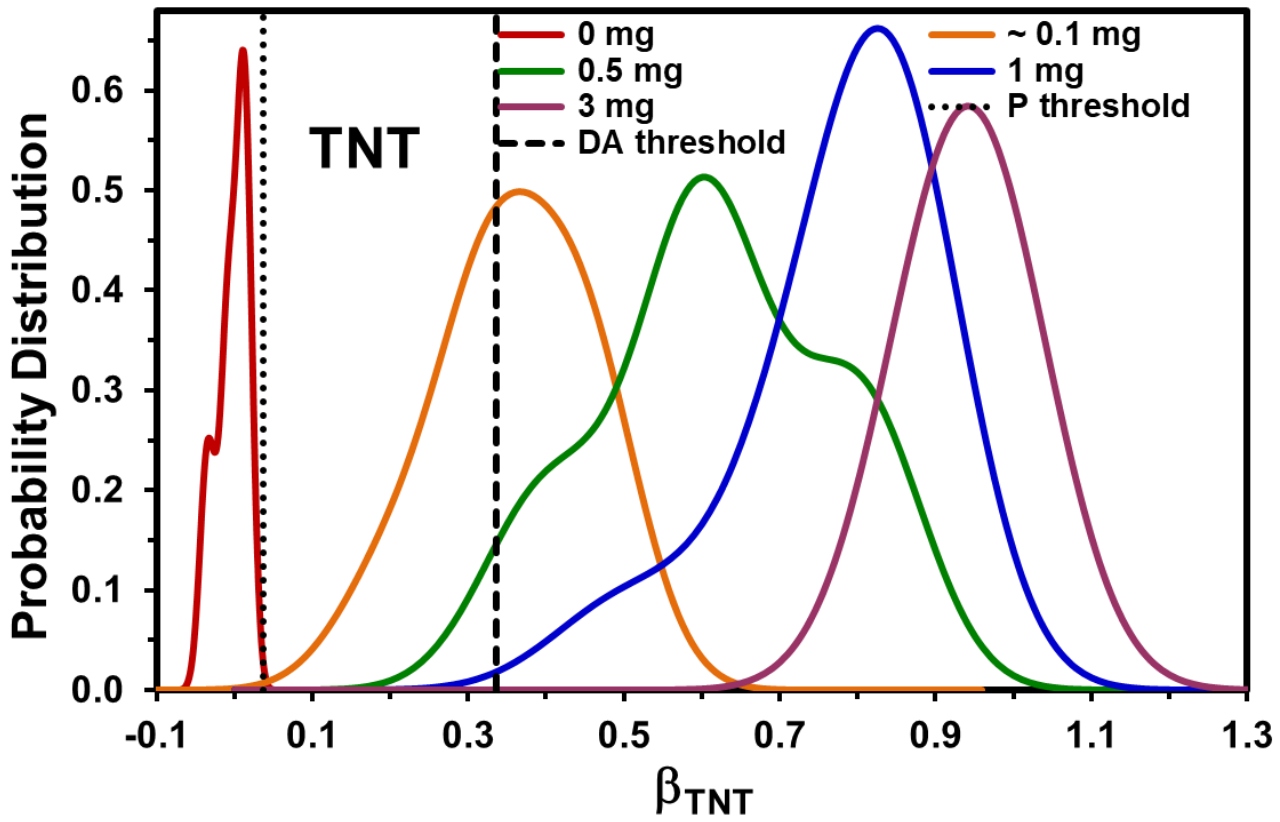

Figure S3. Kernel probability distribution estimation for the $\hat{\beta}_{\mathrm{HE}}$ parameter of TNT ($\hat{\beta}_{TNT}$).

3. CLS Binary Model for PETN/cotton

The binary model for the binary mixture between PETN and cotton consisted of spectra of the neat fabric and spectra of cotton dosed with PETN. The equation is as follows:

$$f_{cotton}^{PETN} = \hat{\beta}_0 + \hat{\beta}_{cotton}\varphi_{cotton}(\omega_i) + \hat{\beta}_{PETN}\varphi_{PETN}(\omega_i) \quad \text{(SM 2)}$$

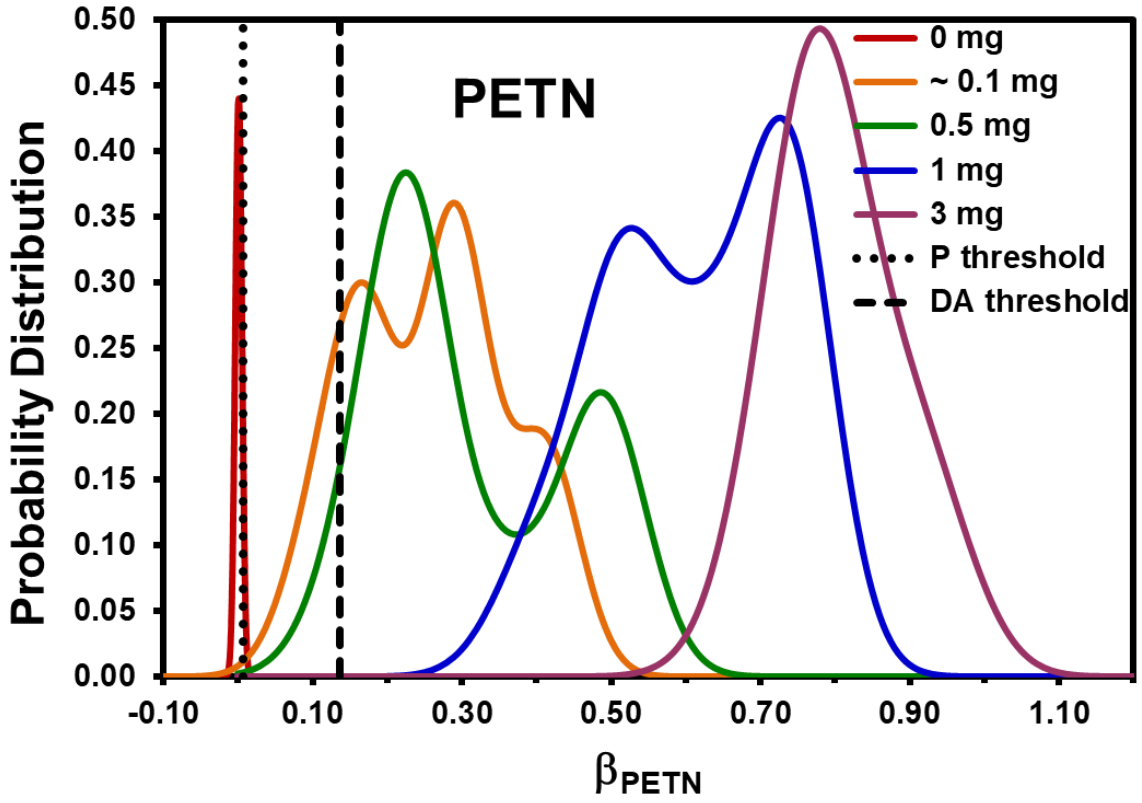

Figure S4. Kernel probability distribution estimation of the $\hat{\beta}_{\mathrm{HE}}$ parameter for PETN ($\hat{\beta}_{PETN}$).

4. **Second CLS Model: Mixtures of three (3) components**

The second CLS model

$$f_{cotton}^{TNT+RDX} = \hat{\beta}_0 + \hat{\beta}_{cotton}\varphi_{cotton}(\omega_i) + \hat{\beta}_{TNT}\varphi_{TNT}(\omega_i) + \hat{\beta}_{RDX}\varphi_{RDX}(\omega_i)$$ (SM 3)

Various amounts from 0.1 to 3 mg (134 samples) of TNT, RDX, and a mixture of 50% TNT and RDX were deposited on cotton. The β_{TNT} and β_{RDX} parameters were calculated, and the distribution values for each sample was plotted from Equation SM 3.

5. **Third CLS Model: Mixtures of four (4) components**

$$f_{cotton}^{TNT+RDX+PETN} = \hat{\beta}_0 + \hat{\beta}_{cotton}\varphi_{cotton}(\omega_i) + \hat{\beta}_{TNT}\varphi_{TNT}(\omega_i) + \hat{\beta}_{RDX}\varphi_{RDX}(\omega_i) + \hat{\beta}_{PETN}\varphi_{PETN}(\omega_i) \quad \text{(SM 4)}$$

Several amount combinations from 0.1 to 3 mg (252 samples) of TNT, RDX, PETN, and a 50% mixture of TNT with RDX (TNT-RDX), 50% TNT with PETN (TNT-PETN), 50% PETN with RDX (RDX-PETN), and a mixture of 33.3% of TNT, PETN, and RDX (TNT-RDX-PETN) were deposited on the cotton substrates. The $\hat{\beta}_{TNT}$, $\hat{\beta}_{RDX}$, and $\hat{\beta}_{RDX}$ parameters values were calculated along with their distribution plots for each sample from the calculated values following Equation SM 5 (Figure S5).

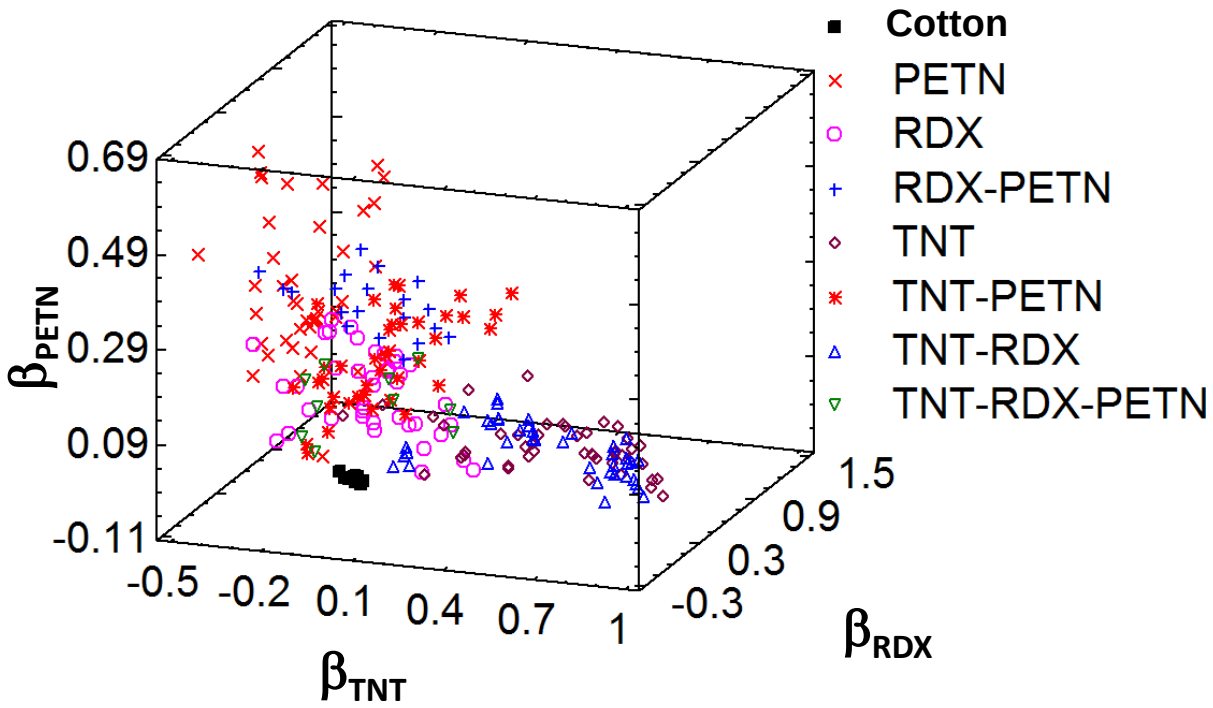

Figure S5. The $\hat{\beta}_{TNT}$, $\hat{\beta}_{RDX}$, and $\hat{\beta}_{PETN}$ parameters samples distribution.

6. Spectra for each HEM and the quaternary mixture

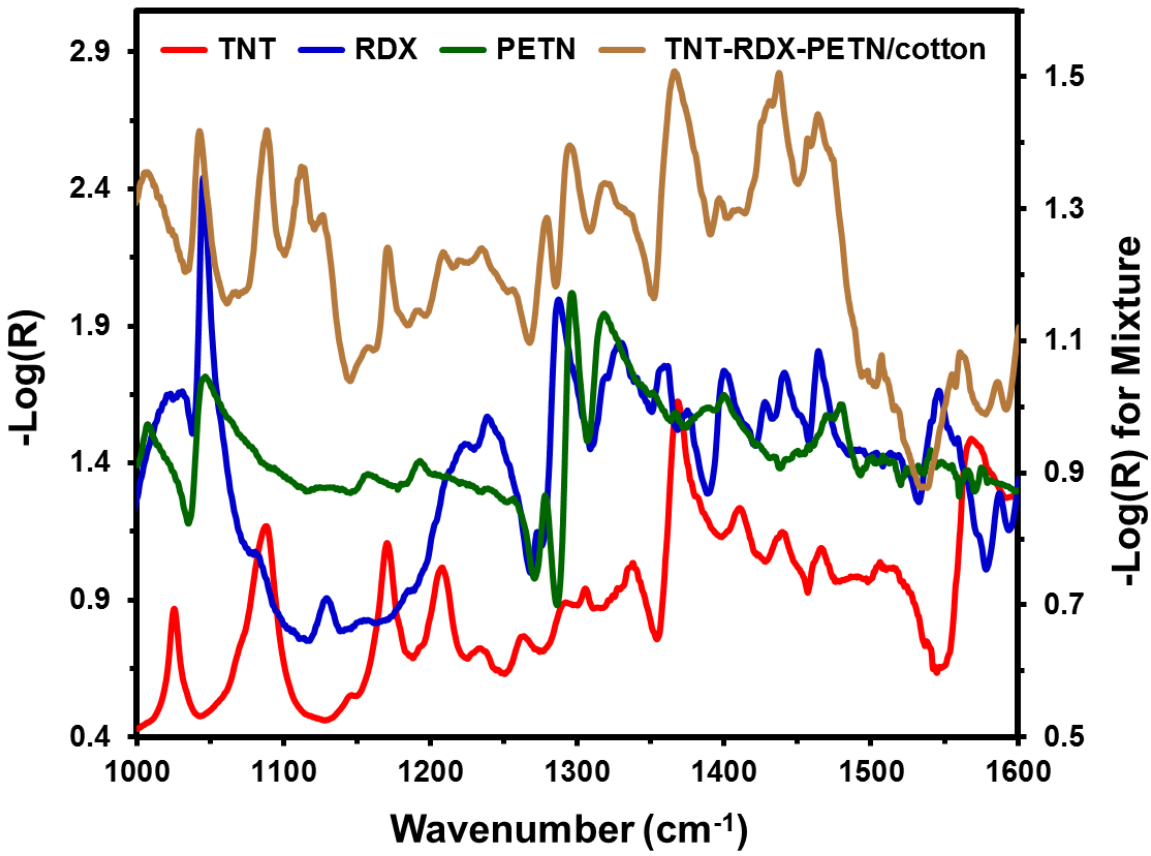

Figure S6. Comparison among HEM spectra and the quaternary mixture spectra.

7. Discriminant Functions Plots

Figures S7 and S8 contain the discriminant function plots for samples of 100% TNT, 100% RDX, and 100% PETN ranging from 0.1 to 3 mg and samples of mixtures of 50% TNT/RDX, 50% TNT/PETN, 50% PETN/RDX, and 33.3% TNT/PETN/RDX with total mass ranging from 0.5 to 3 mg were deposited on cotton fabric substrates (252 samples). In Figure. S8 shows the discrimination achieved when Function 3 is plotted versus Function 1 and in Figure. S8, Function 3 is graphed versus Function 2.

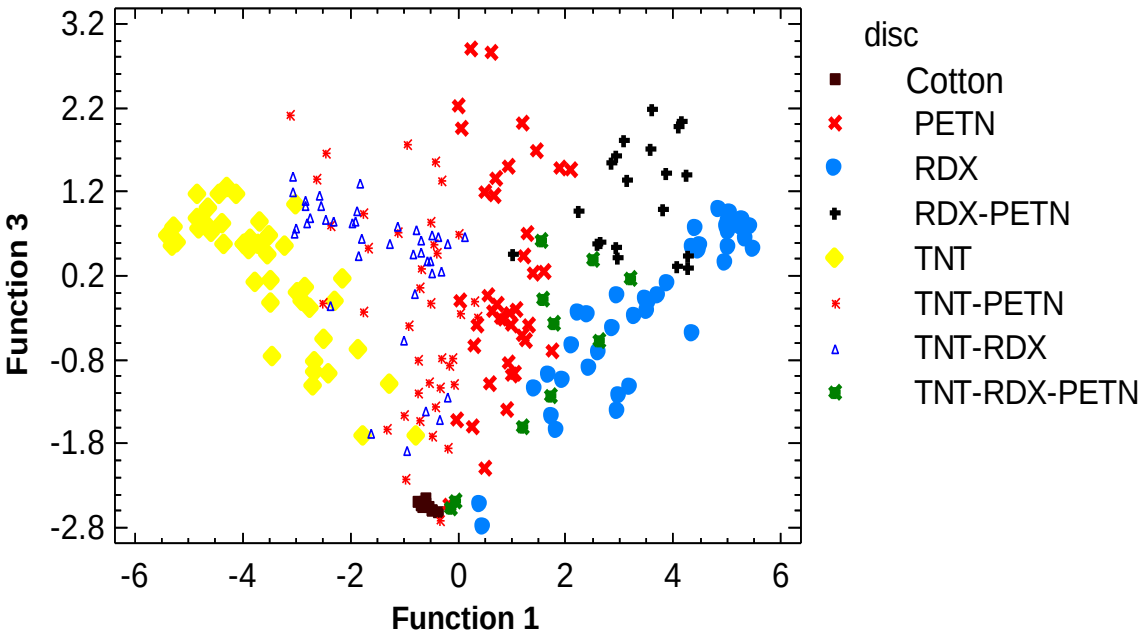

Figure S7. Plot of Discriminant Function 1 versus 3.

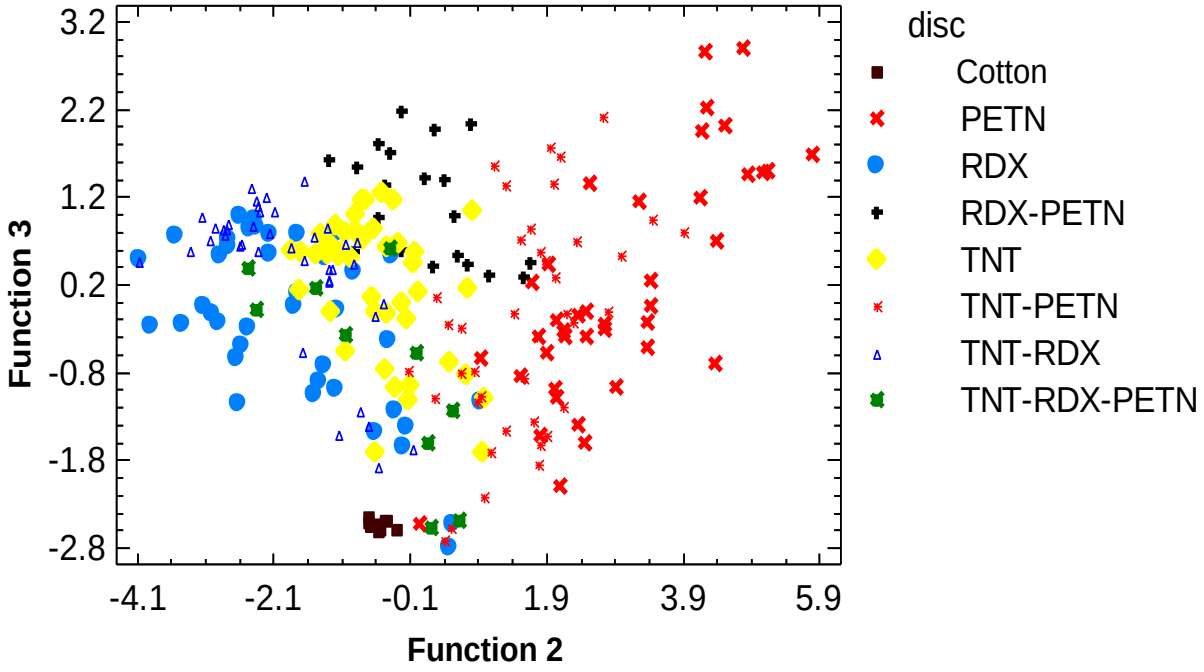

Figure S8. Discriminant Function 2 versus 3.

8. Cotton fabrics substrates: blue jean cotton versus white T-shirt cotton

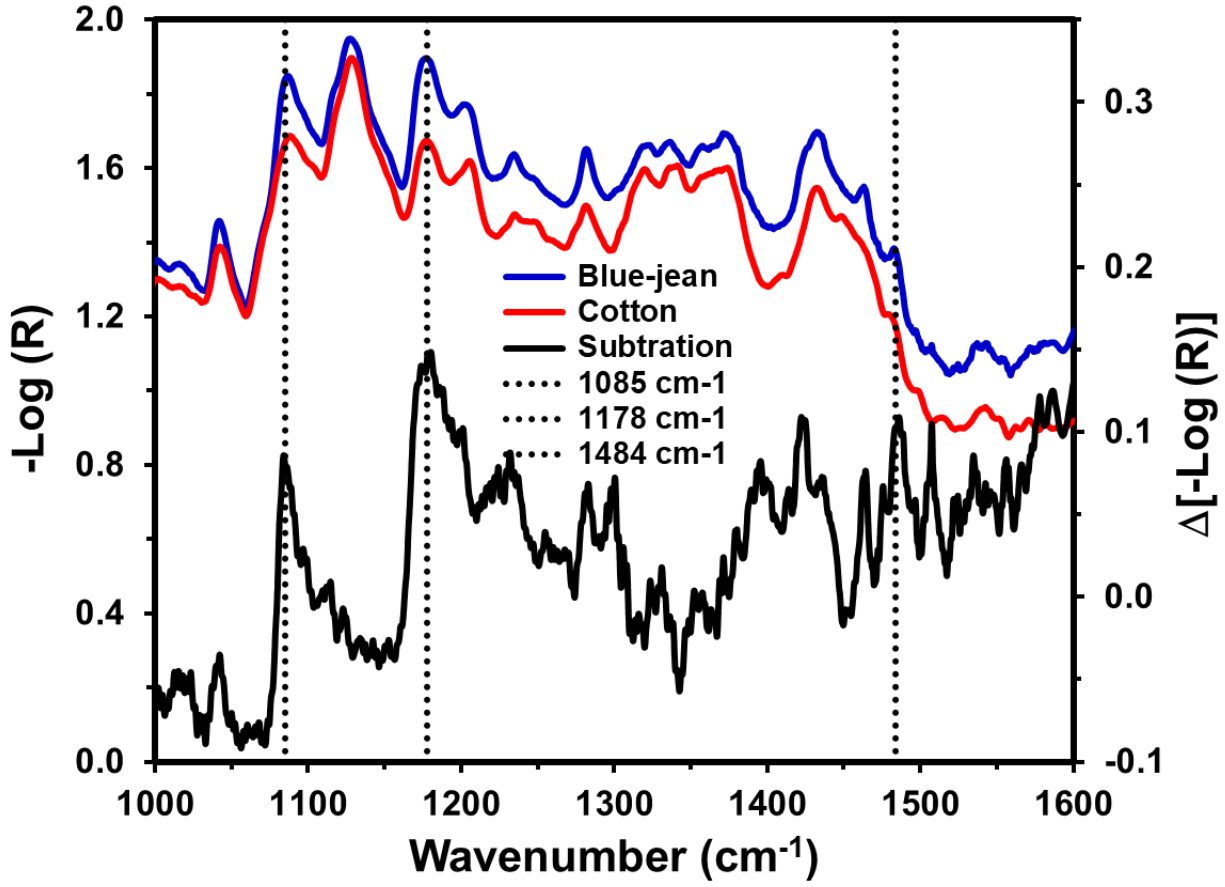

Figure S9. Comparison between cotton from blue jean and cotton; and the difference spectrum.

9. Custom Matlab program to obtain the β parameters for the spectra of the mixtures

```
A = full(file matrix net component); % Loading of matrix of net component
T=full(file mixture);% Loading of matrix of mixture spectra
specwidth=size(A,2); % Number of wavenumber
Ncom=size(A,1); % Number of components
nummix=size(T,1); % Number of mixture
i=1;
X=zeros(Ncom,nummix);% X matrix of fraction for each component for each mixture
mixp=zeros(nummix,specwidth);
while(i<nummix+1) % Calculate the fraction
  C= T(i,:)*A';
  B = A*A';
  p =C/B;
  X(:,i) = p;
  i=i+1;
end
%extract component signals of interest in this case 1 component
for h= 1:nummix
    mix=zeros(1,specwidth);
      for j=2:Ncom
         dumin=X(j,h).*A(j,:);
         mix=mix+dumin;
      end
   mixp(h,:)=mix;
end
D=T-mixp; % extracted matrix
```